AD NUMBER

AD818415

LIMITATION CHANGES

TO:

Approved for public release; distribution is unlimited.

FROM:

Distribution authorized to U.S. Gov't. agencies and their contractors; Critical Technology; NOV 1964. Other requests shall be referred to Air Force Technical Application Center, VELA, Washington, DC 20333. This document contains export-controlled technical data.

AUTHORITY

usaf ltr, 25 jan 1972

(14) EHPA-C73-64(U)9

(6) RADIATION TRANSPORT COMMITTEE REPORT,

by

(10) Harold A. Stewart,
Robert Hopfield
John S. DeGroot

November 25, 1964

(11) 25 Nov-64

(12) 90p

Sponsored by

Advanced Research Projects Agency
Nuclear Test Detection Office
ARPA Order No. 159

Prepared in connection with the VELA-SIERRA program for:

Air Force Technical Application Center
United States Air Force
Washington, D. C.
Contract No. (15) AF33(657)-13599, ARPA Order-159
~~AFTAC Project Authorization No. VT/5061/ASD(59)~~
STATEMENT #2 UNCLASSIFIED

(16) VT/5061

E. H. PLESSET ASSOCIATES, INC.
2444 Wilshire Boulevard
Santa Monica, California

284900

2204

Statement 2. Controlling Office: Hq USAF, attn: AFTAC/VELA, Wash., D.C. 20333. A Healy 15 Aug 67

TABLE OF CONTENTS

1. INTRODUCTION

The Radiation Transport Committee was asked to consider the following:

1. Resonant scattering
2. Excitation transfer
3. Self-reversal
4. Atmospheric transmission
5. Cloud effects
6. Albedo
7. Factors that determine time dependence of signal
8. Solar scintillation

The study of resonant scattering and excitation transfer for the Lyman-Birge-Hopfield series of nitrogen and for the first positive system of nitrogen has been treated by Ed Zipf, whose report is included in Appendix A. Self-reversal, which occurs when an optically thick medium is under consideration, is not important to this discussion because the limiting range for detection of an existing system is one in which the X-ray excitation is so mild that the fluorescent layer behaves an an optically thin medium.

A general discussion of atmospheric effects pertinent to the VELA program is presented below. The material in Section 2 on atmospheric refraction, absorption and scattering in the atmosphere, sky backgrounds, noise in the sky, and reflectivity of the earth's surface is taken from Ref. 1. The material on typical probabilities of signal

modifications by clouds and overcasts is taken from Ref. 2. Work on the earth's albedo, as seen from satellites, and the effects of this on background and time delay of signals was summarized by L. F. Drummeter and incorporated in the Satellite Committee Report. The material presented in Section 2 on the delay of light pulses in overcasts and clouds has been abstracted from a series of reports prepared at E. H. Plesset Associates under AFTAC Contract No. AF 33(657)-13599. The application of these delaying effects to the specific VELA problem is illustrated in Appendix B.

The work on scintillation by G. Milne is presented in Appendix C. The scintillation of an extended source, calculated at E. H. Plesset Associates under AFTAC Contract No. AF 33(657)-13599, is presented in Appendix D and summarized in Section 2 below. Experimental work on the scintillation of the sun, done under the same AFTAC contract at E. H. Plesset Associates, is reported in Appendix E.

2. ATMOSPHERIC EFFECTS

Much of the material on refraction and absorption is taken from Allen.[3] An excellent review of atmospheric refraction is given by Mahan.[4]

2.1 Atmospheric Refraction

The earth is a sphere of radius, $R = 6.37 \times 10^3$ km. The distance D to the geometrical horizon for an observer at height h ($<<R$) is $D^2 \approx 2Rh$ or $D(\text{km}) \approx 3.8 \sqrt{h(\text{meters})}$ or $D(\text{nautical miles}) \approx 1.13 \sqrt{h(\text{ft})}$. A target at h' can just be seen over the horizon by an observer at h and at a distance $D' = \sqrt{2Rh} + \sqrt{2Rh'}$. Refractive effects can modify these results by approximately $\pm$ 20% in D.

Values of $(n - 1) \times 10^6$ for various λ and for p = 760 mm Hg, $t = 0^\circ C$ and f(water vapor pressure) = 4 mm Hg are given by Table I.

Table 1 -- Index of Air as a Function of Wavelength

λ (μ)	0.20	0.24	0.28	0.32	0.36	0.40	0.50	0.60	0.70	0.80
$(n-1) \times 10^6$	340.0	321.2	310.9	304.9	300.9	298.2	294.1	292.0	290.7	290.0

λ (μ)	0.90	1.0	1.2	1.4	1.6	1.8	2.0	3.0	4.0	∞ optical
$(n-1) \times 10^6$	289.4	289.0	288.6	288.3	288.1	288.0	287.9	287.7	287.6	287.5

The combination of the altitude gradient in refractive index and the earth's curvature result in a deviation of the light from stars and a limitation on the air mass between star and ground observer as shown in Table II.

Table II -- Refraction and Air Mass

Refraction and air mass. The table shows the relation between refraction and apparent zenith distance z; it also gives the air mass which for small z is equal to $\sec z$. The values are tabulated for $p = 760$ mm·Hg and $t = 10$ °C ; for other values of p and t multiply both the air mass and the refraction $R = \zeta - z$ by $p/760(0.002 + 0.0038t)$.

Apparent altitude $h = 90° - z$	True zenith distance ζ	$\sec z$	Air mass [3, 9]
0°	90° 35′ 21″	∝	38
1°	89° 24′ 45″	57·30	26·96
2°	88° 18′ 24″	28·65	19·79
3°	87° 14′ 24″	19·11	15·36
4°	86° 11′ 43″	14·34	12·44
5°	85° 9′ 51″	11·47	10·40
6°	84° 8′ 27″	9·567	8·900
7°	83° 7′ 23″	8·206	7·768
8°	82° 6′ 33″	7·185	6·884
9°	81° 5′ 52″	6·392	6·177
10°	80° 5′ 18″	5·759	5·600

Apparent altitude $h = 90° - z$	True zenith distance ζ	$\sec z$	Air mass [3, 9]
10°	80° 5′ 18″	5·759	5·600
15°	75° 3′ 34″	3·864	3·816
20°	70° 2′ 38″	2·924	2·904
25°	65° 2′ 4″	2·366	2·357
30°	60° 1′ 41″	2·000	1·995
40°	50° 1′ 10″	1·556	1·553
50°	40° 0′ 49″	1·305	1·304
60°	30° 0′ 34″	1·155	1·154
70°	20° 0′ 21″	1·064	1·064
80°	10° 0′ 10″	1·015	1·015
90°	0° 0′ 0″	1·000	1·000

Crude calculations of altitude dependence of pressure to about 120 km may be made using the height of the homogeneous atmosphere H as a value for scale height $p_h = p_o^{-h/H}$ where H is related to ground temperature as shown in Table III.

Table III -- Height of the Homogeneous Atmosphere

Ground Temp. °C	-30	-15	0	+15	+30
H in km	7.113	7.552	7.991	8.43	8.869

Reasonable calculations of altitude dependence of temperature, t_h up to the tropopause may be made as follows: $t_h = t_o - (t_o - t_h)\, h/h_t$. The variation of tropopause height, h_t, and temperature t_t with changing latitude is shown in Table IV.

Table IV -- Height of the Tropopause

Variation of Meteorological Quantities with Latitude

The table averages the Northern and Southern hemispheres which differ in detail as a result of the different land distributions

Latitude	Mean air temperature (sea-level)	Seasonal temperature range (on land)	Ocean temperature	Total pressure (sea-level)	Water-vapour pressure (sea-level)	Tropopause		
						temperature	height	pressure
	°C	°C	°C	mm-Hg	mm-Hg	°C	km	mm-Hg
0°	27	1	27	758	21	−67	17·8	69
10°	26	3	26	759	20	−80	16·5	73
20°	24	6	24	761	18	−73	14·8	97
30°	20	9	20	763	14	−66	12·9	127
40°	13	13	14	761	9	−62	11·2	160
50°	6	17	7	756	5	−58	9·7	198
60°	−2	21	2	761	2	−55	8·5	233
70°	−10	26	0		1	−54	7·8	258
80°	−18	29	−2			−53	7·0	285
90°	−25							

2.2 Absorption in the Atmosphere

The specular transmission through a homogeneous atmosphere T_λ of monochromatic light of wavelength λ over equivalent path length L in cm at STP is given by

$$T_\lambda = \exp-(K_\lambda + \sigma_\lambda)L \qquad (1)$$

where K_λ is the absorption coefficient and σ_λ is the scattering coefficient. Small wavelength intervals in the ultraviolet and visible may be treated by Eq. (1) and values of K_λ are given in Figure 1. Appropriate values of L may be derived from Figure 2.[5] In cases of N_2, O_2, O_3 and H_2O the composition of unit atmosphere in cm thicknesses at STP are 624,600, 167,600, 0.3 and from 300 to 5000 respectively.

In the infrared the rotational structure of the absorption spectra of atmospheric molecules is, in general, not resolved and the assumption that K_λ is nearly constant over a small wavelength interval is not valid. Under these conditions the transmission is described by Eq. (2).

$$T_\lambda = f(b_\lambda \ell) \exp(-\sigma_\lambda L) \qquad (2)$$

Ultra-violet Absorption of Atmospheric Gases

The diagram gives $\log k_\lambda$, where k_λ is the exponential absorption coefficient per atmo-cm (i.e. per cm at S.T.P.). In order to determine atmospheric absorption from the curves it would be necessary to allow for atmospheric composition and the degree of dissociation of some molecules. In the region 900 A to 1000 A there are two curves for O_2. Of these the curve representing the highest absorption allows for the pre-ionization factor

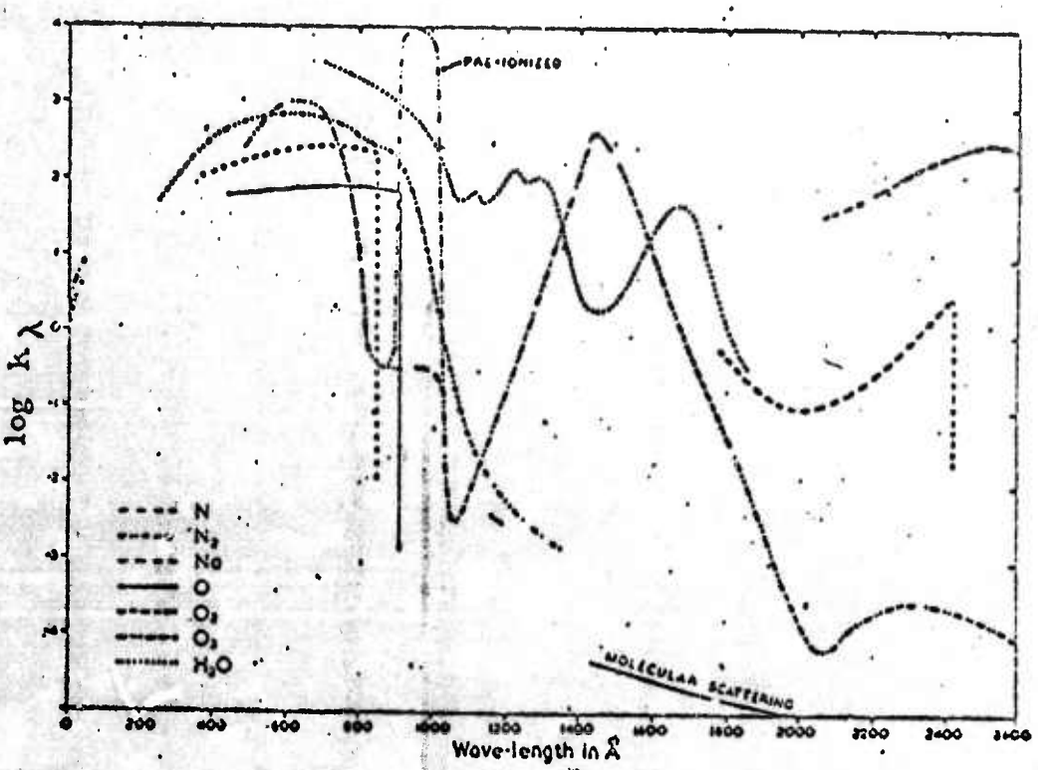

Ultra-violet absorption of atmospheric gases

Figure 1 (from ref. 3)

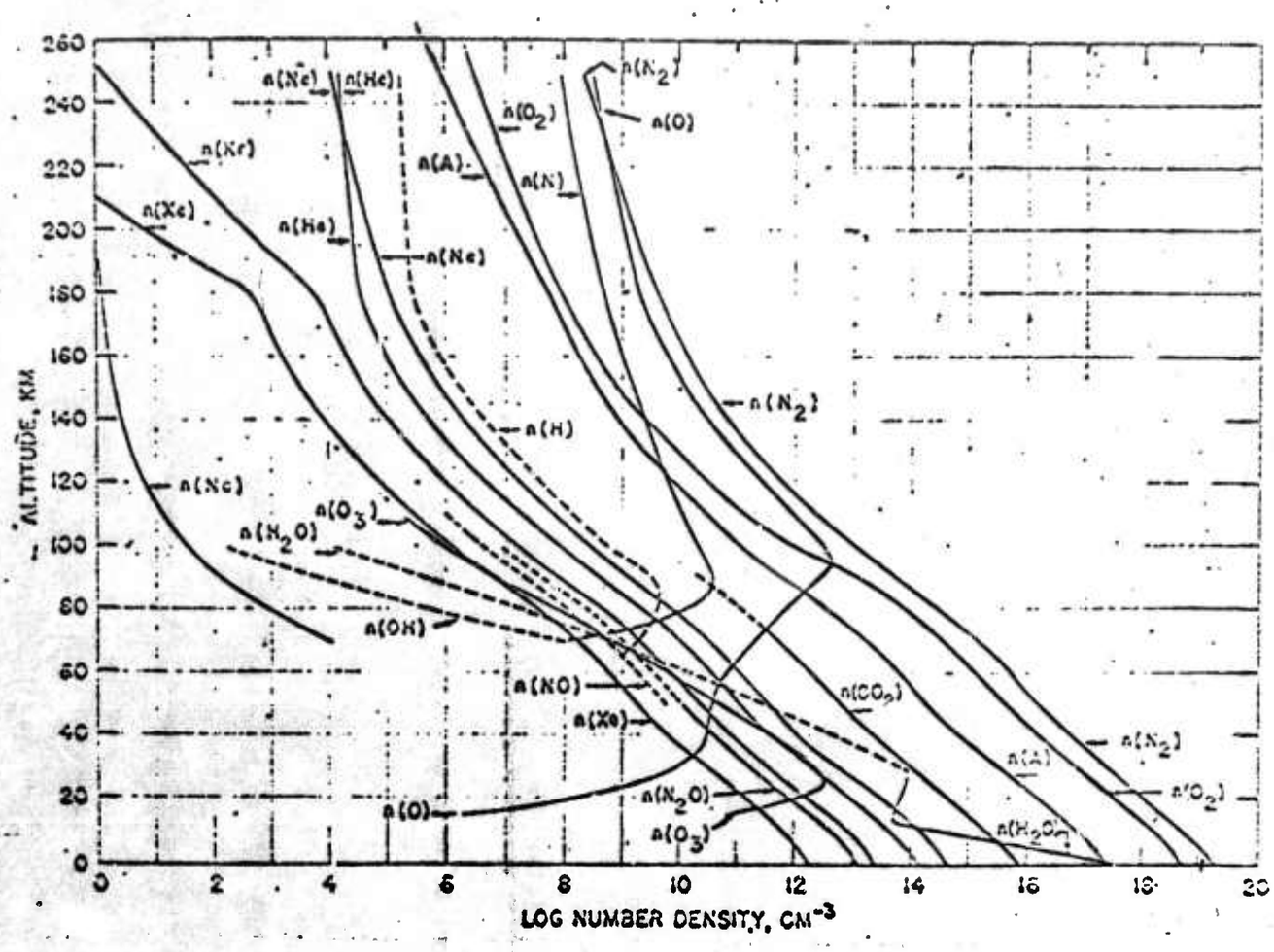

Figure 2 (from ref. 5)

where $f(b_\lambda l)$ is given in Table V and values for $\log b_\lambda$ are shown in Figures 3 and 4. Here l corresponds to the values of b_λ for unit air mass.

Table V -- Band Absorption of Atmospheric Gases

Bands made up of discrete lines will not obey the Lambert law of exponential absorption and the absorption coefficient must be replaced by its analogue b_λ such that the transmission is $f(b_\lambda l)$ where l is the layer thickness in some appropriate unit. For the function f we adopt the relation given below:

$\log(b_\lambda l)$	$f(b_\lambda l)$
−3·0	1·000
−2·5	0·990
−2·0	0·971
−1·8	0·958
−1·6	0·940
−1·4	0·914

$\log(b_\lambda l)$	$f(b_\lambda l)$
−1·2	0·897
−1·0	0·836
−0·8	0·782
−0·6	0·721
−0·4	0·651
−0·2	0·578

$\log(b_\lambda l)$	$f(b_\lambda l)$
0·0	0·500
+0·2	0·412
+0·4	0·332
+0·6	0·258
+0·8	0·187
+1·0	0·124

$\log(b_\lambda l)$	$f(b_\lambda l)$
+1·2	0·072
+1·4	0·033
+1·6	0·011
+1·8	0·001
+2·0	0·000

Except for the Chappuis, the Huggins, and the Hartley bands of O_3 there is little significant absorption in the atmosphere between 0.3 μ and 0.7 μ. (See Table VII).

2.3 Scattering in the Atmosphere

The Rayleigh equation describes the inescapable scattering in the atmosphere due to its molecular constituents. At STP the value of σ_λ appropriate for use in Eqs. (1) and (2) is never less than $\sigma_\lambda = 1.07 \times 10^{-3} \lambda^{-4.05}$ km^{-1} (λ in μ). Such clear air has not been observed experimentally since the atmosphere supports water droplets (fog, haze, clouds), ice crystals and dust. The distance at which a large black object can just be seen against the horizon in daytime is called the visual or meterological range and this distance is dependent upon the concentration of scattering centers in the atmosphere. A rough but useful relationship between σ_λ (km^{-1}), visual range V(km) and wavelength $\lambda(\mu)$ is [6]

$$\sigma_\lambda = \frac{3.9}{V} \left(\frac{0.53}{\lambda}\right)^{+.62V^{1/3}}$$

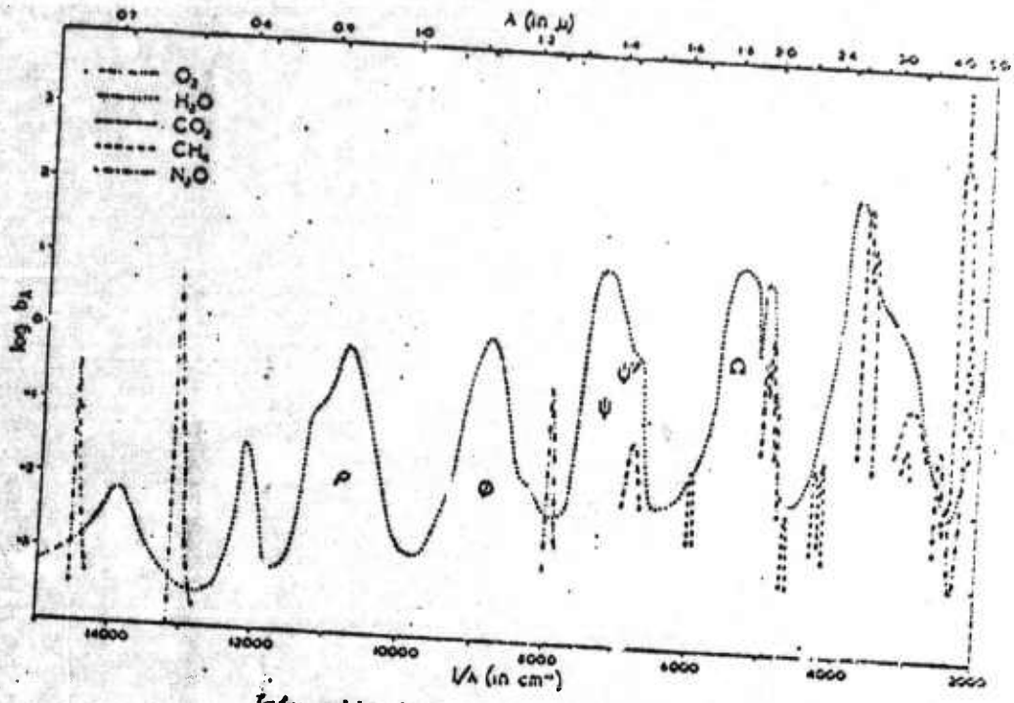

Infra-red band absorption of atmospheric gases

The quantity b_λ is the reciprocal of the thickness (in the units chosen) that would give 50% absorption.

The values of $\log b_\lambda$ for individual atmospheric gases are given in the diagrams.

The unit chosen for l is an amount normally found in 1 air mass, as follows

for H_2O	unit of l =	1 245	atmo-cm = 1 cm	precipitable water
O_2	" =	167 600	"	
O_3	" =	0·3	"	
CO_2	" =	220	"	
N_2O	" =	0·4	"	
CH_4	" =	1·2	"	

Figure 3 (from ref. 3)

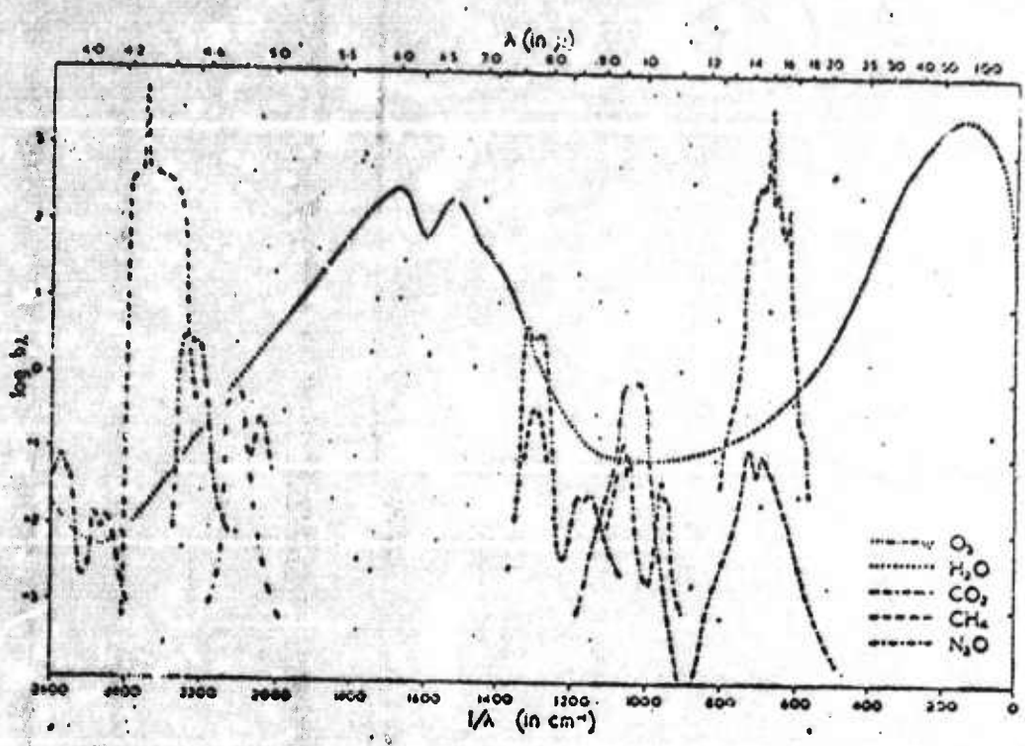

Infra-red band absorption of atmospheric gases

Figure 4 (from ref. 3)

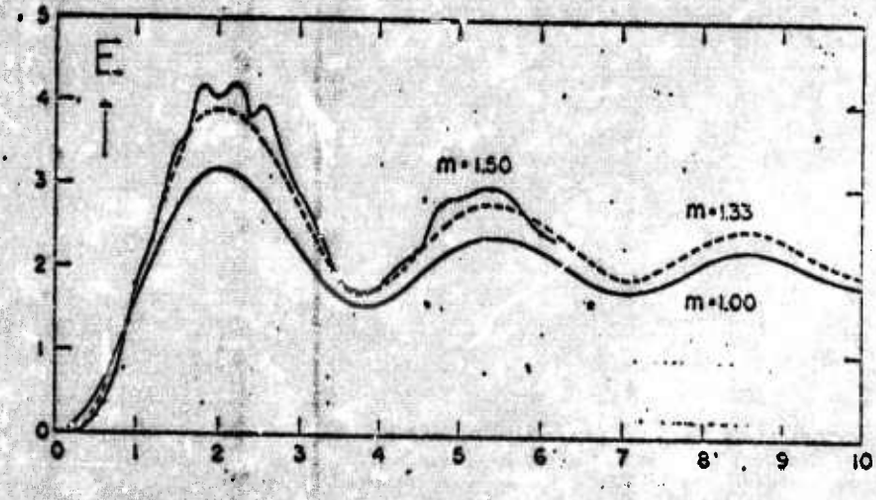

—The efficiency factor, E, for extinction by small spheres as a function of the size parameter, x, and the refractive index, m.

Figure 5 (from ref. 7)

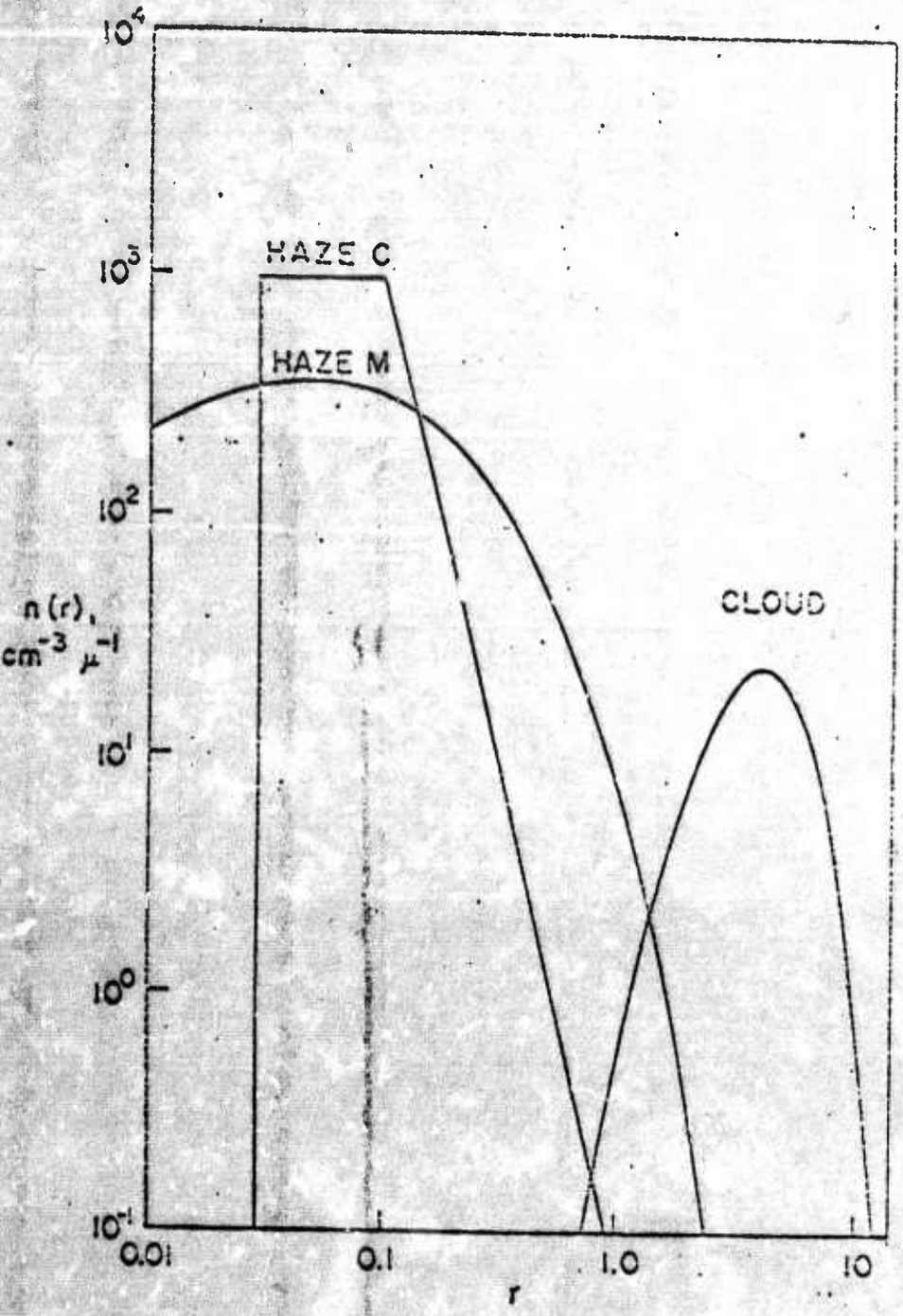

Three Size Distribution Functions Used in the Ingegration of the Mie Functions. Total Concentration 100/cm^3

Figure 6 (from ref. 8)

Figure 7

(from ref. 9)

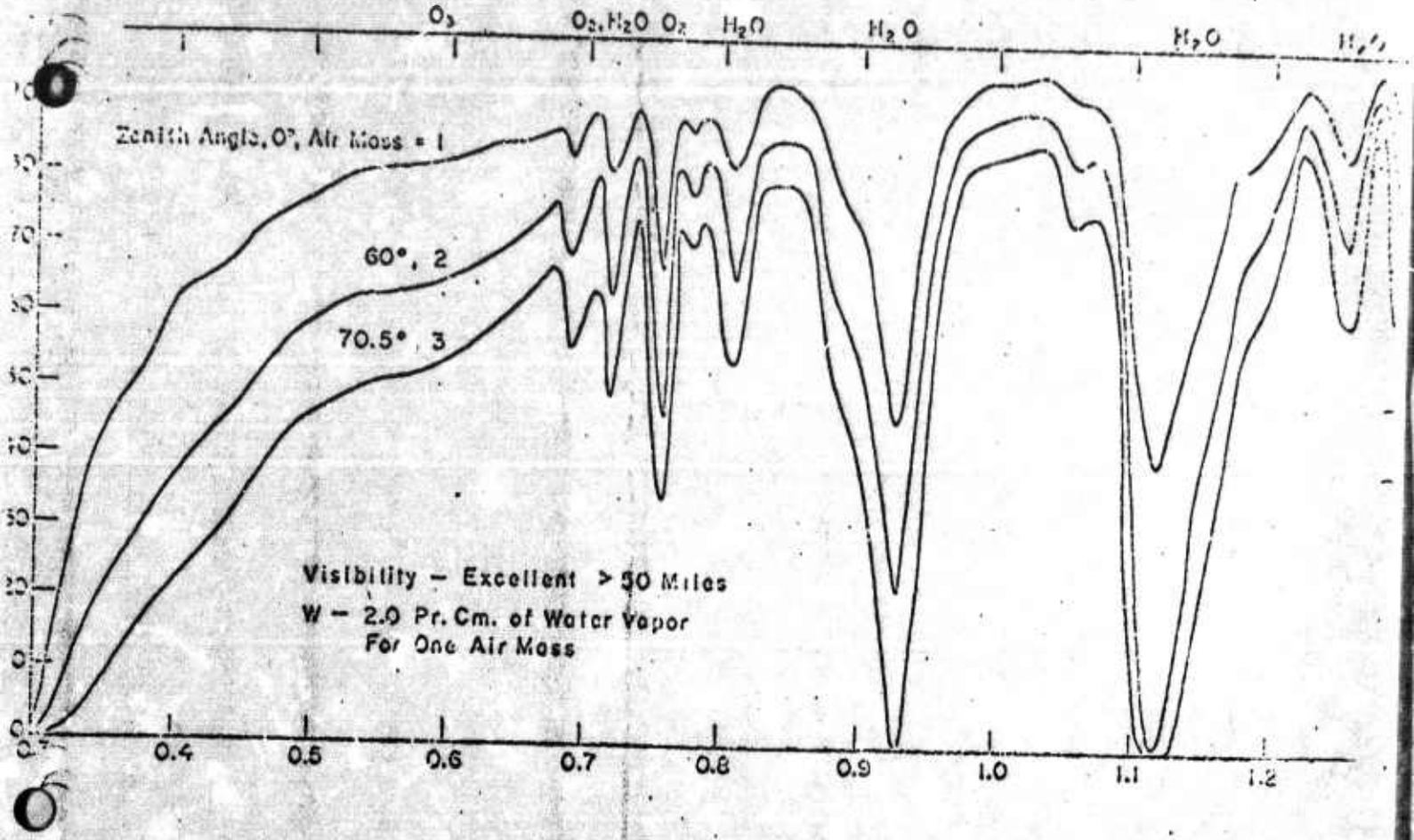

Figure 8

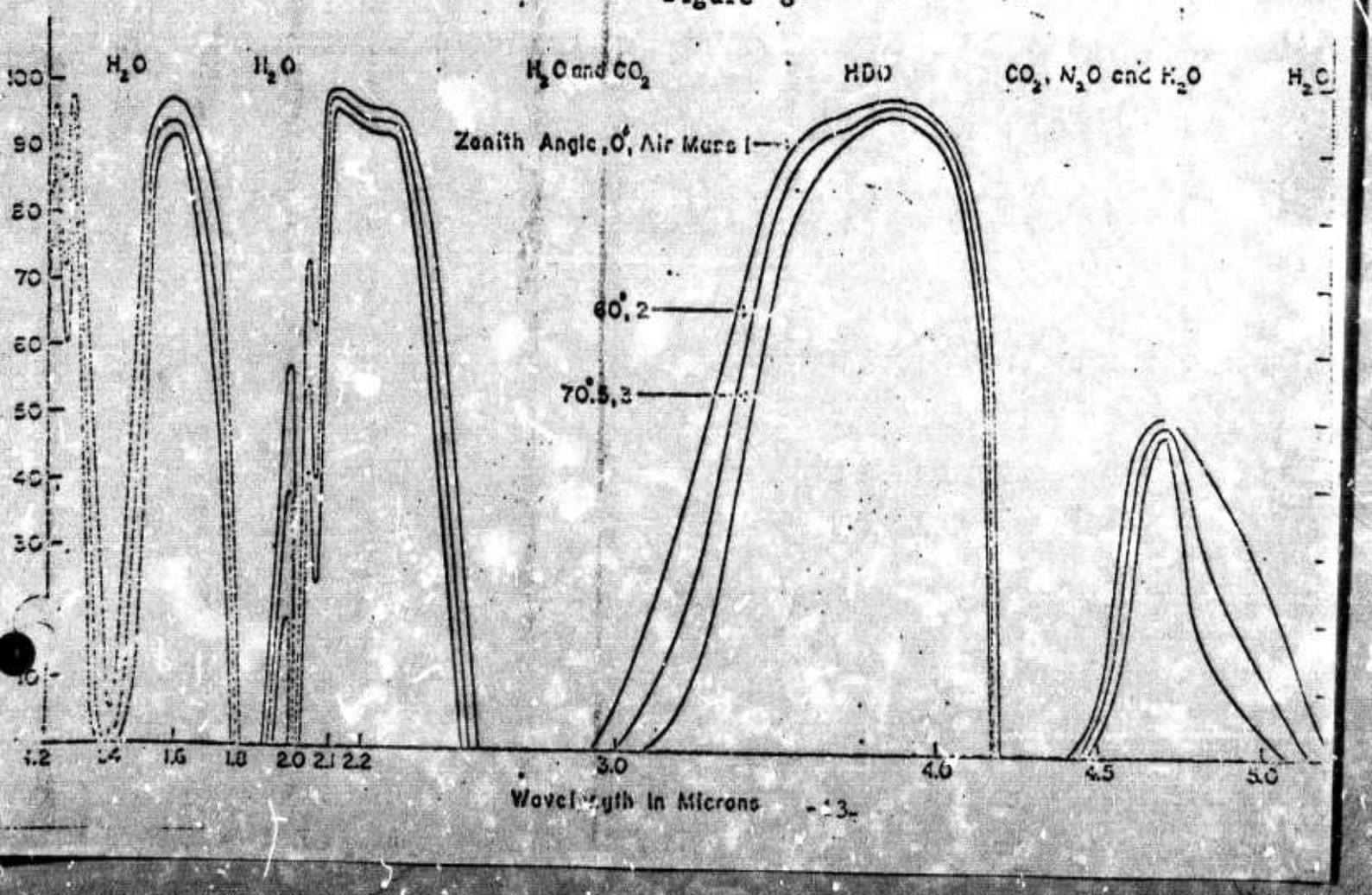

Table VII -- Continual Atmospheric Absorption

λ	Molecular scattering	Water-vapour	Ozone	Dust, fairly clear conditions	Total	Transmission
μ	per atmosphere	per cm precipitable water	per 3 mm at S.T.P.	per atmosphere		
0·20	7·26			0·24	20 ?	0·00
0·22	4·68		19	·21	27	0·00
0·24	3·16		65	·19	68	0·00
0·26	2·21		88	·17	89	0·00
0·28	1·606		36	·157	38	0·00
0·30	1·194		3·2	·143	4·5	0·011
0·32	0·908		0·25	·132	1·30	0·272
0·34	0·702	0·010	0·02	·122	0·84	0·43
0·36	0·552	·006	0·00	·113	0·67	0·51
0·38	0·441	·0044	0·00	·106	0·55	0·58
0·40	0·356	·0030	0·00	·099	0·46	0·63
0·45	0·219	·0031	0·001	·084	0·31	0·73
0·50	0·142	·0025	0·012	·074	0·23	0·795
0·55	0·096	·0022	0·031	·065	0·19	0·827
0·60	0·0675	·0020	0·044	·058	0·17	0·844
0·65	0·0488	·0017	0·023	·053	0·127	0·881
0·70	0·0361	·0014	0·008	·048	0·093	0·911
0·80	0·0211	·0012	0·001	·040	0·063	0·939
0·90	0·0131	·0011	0·00	·035	0·049	0·952
1·0	0·0086	·0010		·030	0·040	0·961
1·2	0·0041	·0010		·024	0·029	0·971
1·4	0·0022	·0010		·019	0·022	0·978
1·6	0·0013	·0010		·016	0·018	0·982
1·8	0·0^3 80	0·0010		·014	0·016	0·984
2·0	0·0^3 53			·012	0·013	0·987
3·0	0·0^3 10			·007	0·007	0·993
4·0	0·0^3 33			0·005	0·005	0·995

2.4 Sky Backgrounds

The atmosphere scatters sunlight, moonlight and starlight so that for wavelengths in excess of 0.3 microns (the ozone cutoff) there is a smoothly varying brightness over the whole sky. In addition to this scattered light there is a background observable at night which is due to other sources as listed.[10]

Zodiacal	15%
Galactic	5%
Luminescence of night sky	40%
Scattering from the above	10 %
Plus starlight direct and scattered	30%

Rayleigh scattering causes polarization of skylight. The phase functions for Rayleigh scattering of unpolarized light are given as $f_{\perp}(\theta) = \frac{3}{16\pi}$ and $f_{11}(\theta) = \frac{3}{16\pi}\cos^2\theta$ where $\perp$ and 11 describe the state of polarization in the plane of scattering. Hence the light scattered into unit solid angle at angle θ from unit volume containing m scattering centers and illuminated by I_0 is $I_\theta = I_0 \quad \sigma\left[f_{\perp}(\theta) + f_{11}(\theta)\right] = I_0 \frac{3\sigma}{16\pi}(1 + \cos^2\theta)$ (per steradian).

For the molecular scattering in the atmosphere this is approximately correct, and, with the reservations pointed out by van der Hulst,[11] one may write $I_\theta = I_0 \frac{3}{16\pi}(1 + \cos^2\theta)\,(1.07 \times 10^{-8}\lambda^{-4.05})$ (per cubic cm pure air at STP).

Rayleigh polarization is illustrated in Figure 9.

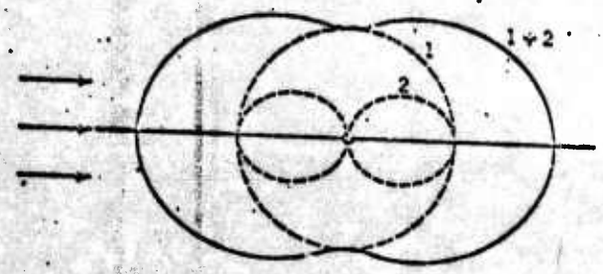

Rayleigh scattering: polar diagram of scattered intensity if incident radiation is unpolarized. 1 = polarized with electric vector $\perp$ plane of drawing. 2 = polarized with electric vector in plane of drawing. 1 + 2 = total.

Figure 9 (from ref. 7)

The aerosols in the atmosphere in general produce strong forward scattering and some polarization. The phase functions for continental and maritime haze and for clouds are shown in Figure 10 a, b, and c, respectively.[8] As a generalization, the sky brightness above the tropopause can be calculated on the basis of the Rayleigh scattering phase function increased by a factor of 1.3. This sometimes holds above an inversion, and infrequently at ground level. For the conditions in which the single scattering approximation is

Figure 10 a, b, c (from ref. 8)

Normalized scattering phase functions for several atmospheric conditions. (Note: to find polarization independent values, take average of two curves rather than sum).

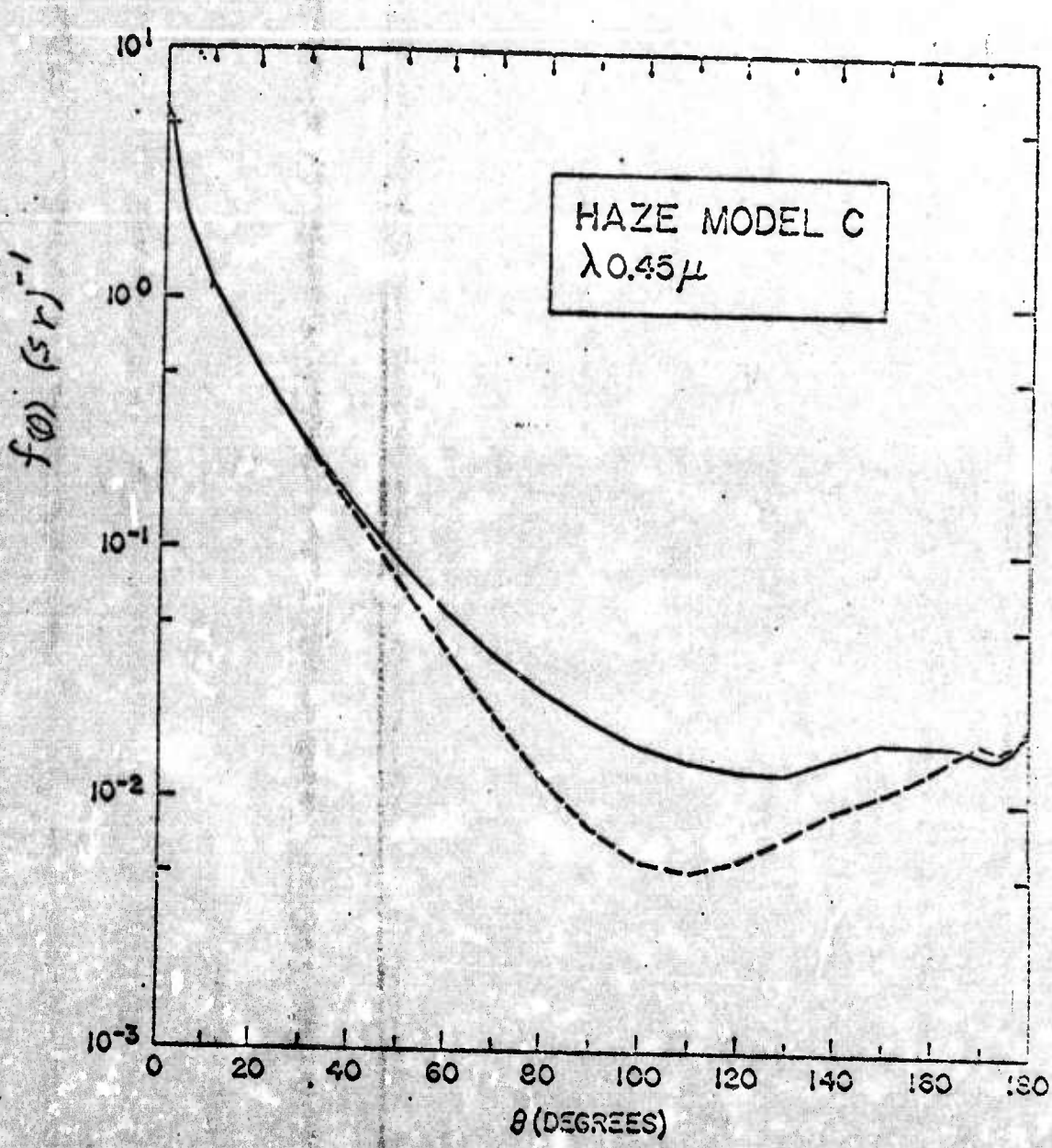

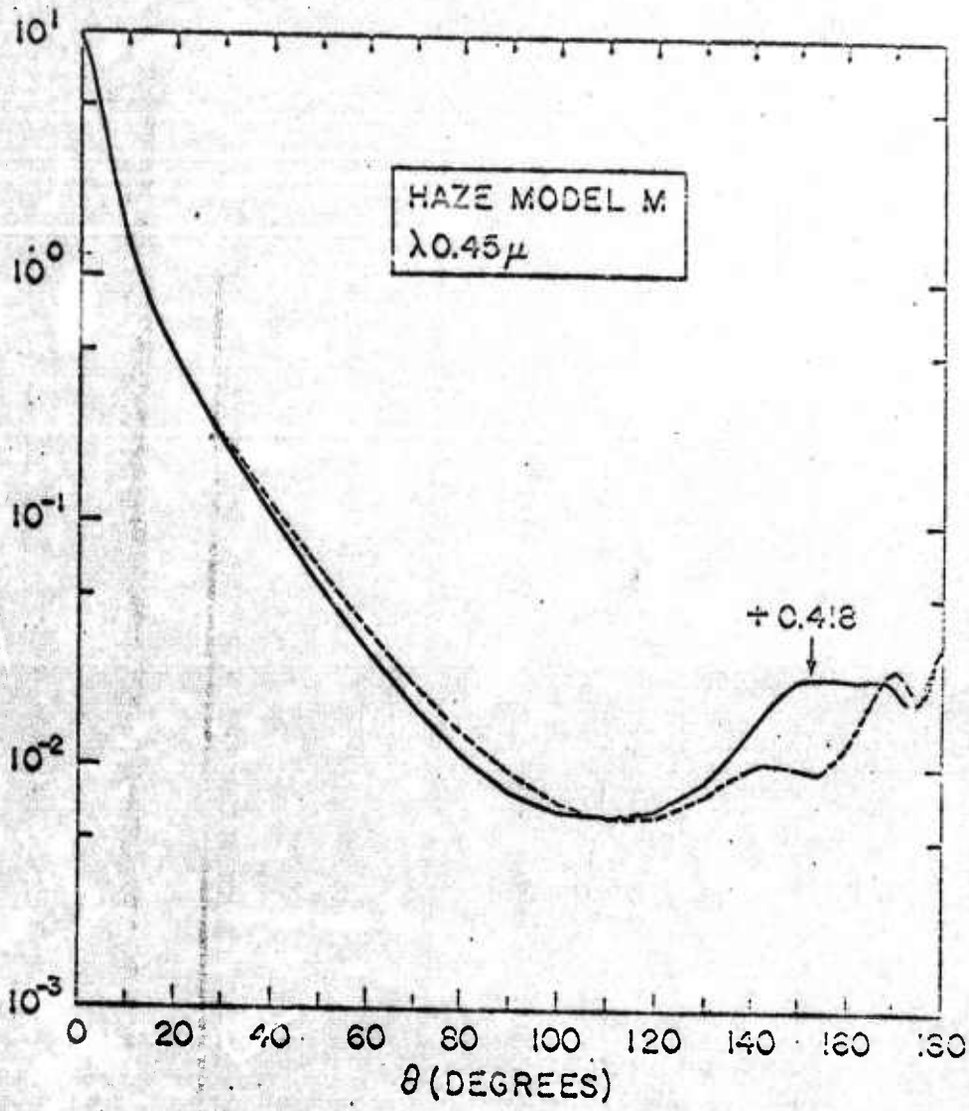
HAZE MODEL M
λ0.45μ
+0.418
10^{1}
10^{0}
10^{-1}
10^{-2}
10^{-3}
0
20
40
60
80
100
120
140
160
180
θ (DEGREES)
f(θ) (sr)$^{-1}$

Figure 10b

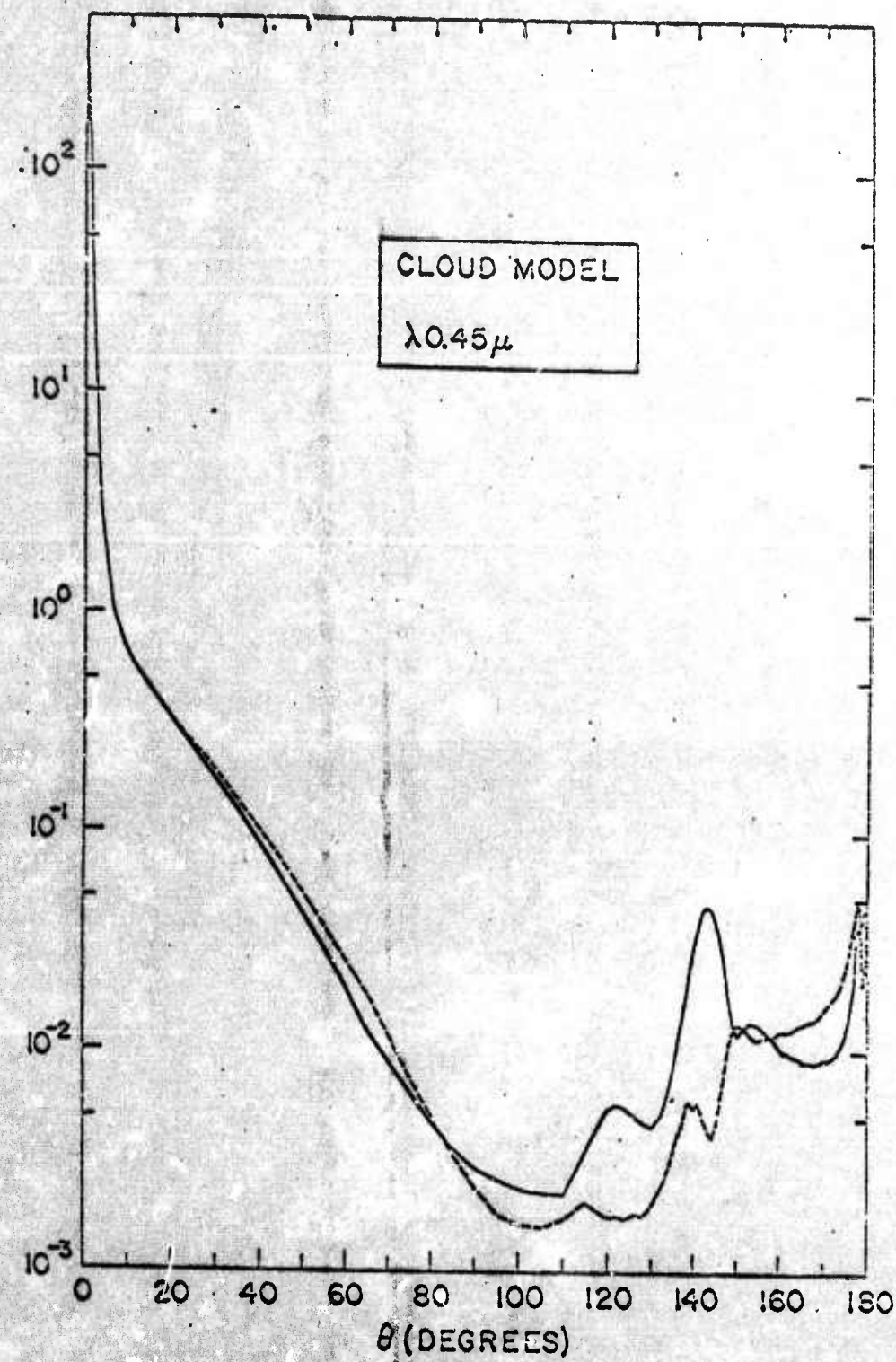
CLOUD MODEL
λ0.45μ
10^2
10^1
10^0
10^{-1}
10^{-2}
10^{-3}
$i(\theta)$ (sr)$^{-1}$
0
20
40
60
80
100
120
140
160
180
θ (DEGREES)

Figure 10c

acceptable (total path length in atmosphere less than σ^{-1}) spectral sky brightness values are given by $I(\theta, z, \lambda) = I_{0(\lambda)} \sigma_\lambda H(\sec z) f(\theta)$ watt cm^{-2} sr^{-1} μ^{-1}, where $I_{0(\lambda)}$ is incident sunlight in watts cm^{-2}, z is angle from zenith to line of sight, θ is angle through which sunlight is scattered toward detector.

The transmission or reflection coefficients of uniform overcasts and the reflection characteristics of large plane surfaces of clouds can be treated with considerable accuracy through the use of the following equations. The transmission, T, of the overcast for light incident at an angle θ to the overcast normal is

$$T = \frac{1 + (\cos \theta - .5)(1 - e^{-D/\lambda \cos \theta})}{1 + D/\lambda}$$

where

D is the thickness of the overcast,
λ is the transport mean free path,
$\lambda = \lambda_s/(1-\bar{\mu}_o)$,
λ_s is the scattering mean free path in the overcast,
$\bar{\mu}_o$ is the average cosine of the scattering angle.

Hence, for light incident at an angle $\theta = 60^\circ$ the transmission is

$$T_{60^\circ} = 1/1 + (D/\lambda) \qquad (3)$$

The normalized distribution in angle of the transmitted light is made up of two parts. One part is from the light which was scattered within the overcast. The other is from the non-scattered light, which is specular. The specular component is proportional to $e^{-D/\lambda_s \cos \theta}$.

The scattering in an overcast is very forward, i.e.,

$$\lambda \gg \lambda_s .$$

Therefore, even for $T_{60^\circ} = .5$ (a rather thin overcast), the factor D/λ_s is quite large; hence, the unscattered component may be ignored. In this case the distribution in angle of the transmitted light is

$$f(\phi) = (3/7\pi)(1+2\cos\phi)$$

where

ϕ is the angle to the normal of the overcast
$f(\phi)$ is the normalized distribution, 1/steradian, i.e.,

$$2\pi \int_0^{\pi/2} f(\phi) \cos\phi \sin\phi \, d\phi = 1$$

Also, the amount of light reflected is given by $R = 1 - T$, or

$$R = \frac{(D/\lambda) - (\cos\theta - .5)(1 - e^{-D/\lambda \cos\theta})}{1 + (D/\lambda)}$$

And this light is distributed in angle according to $f(\phi)$.

The transmission of light as a function of time was calculated using diffusion theory.

Shown in Figure 11 is the probability of transmission of the scattered light, P, by an overcast, as a function of time for various overcast thicknesses. The source is an instantaneous pulse of radiation incident at an angle of 60° to the normal at t = 0. The probability of transmission of the scattered light as a function of time is normalized so that the integral, P, over all time is as follows:

$$T = \int_0^\infty P \, dt + e^{-D/\lambda \cos\theta}$$

Figure 11

Probability of Transmission of an Overcast Vs. Time for Various Overcast Thicknesses

Source is an instantaneous pulse incident at 60° to the normal at time = 0.

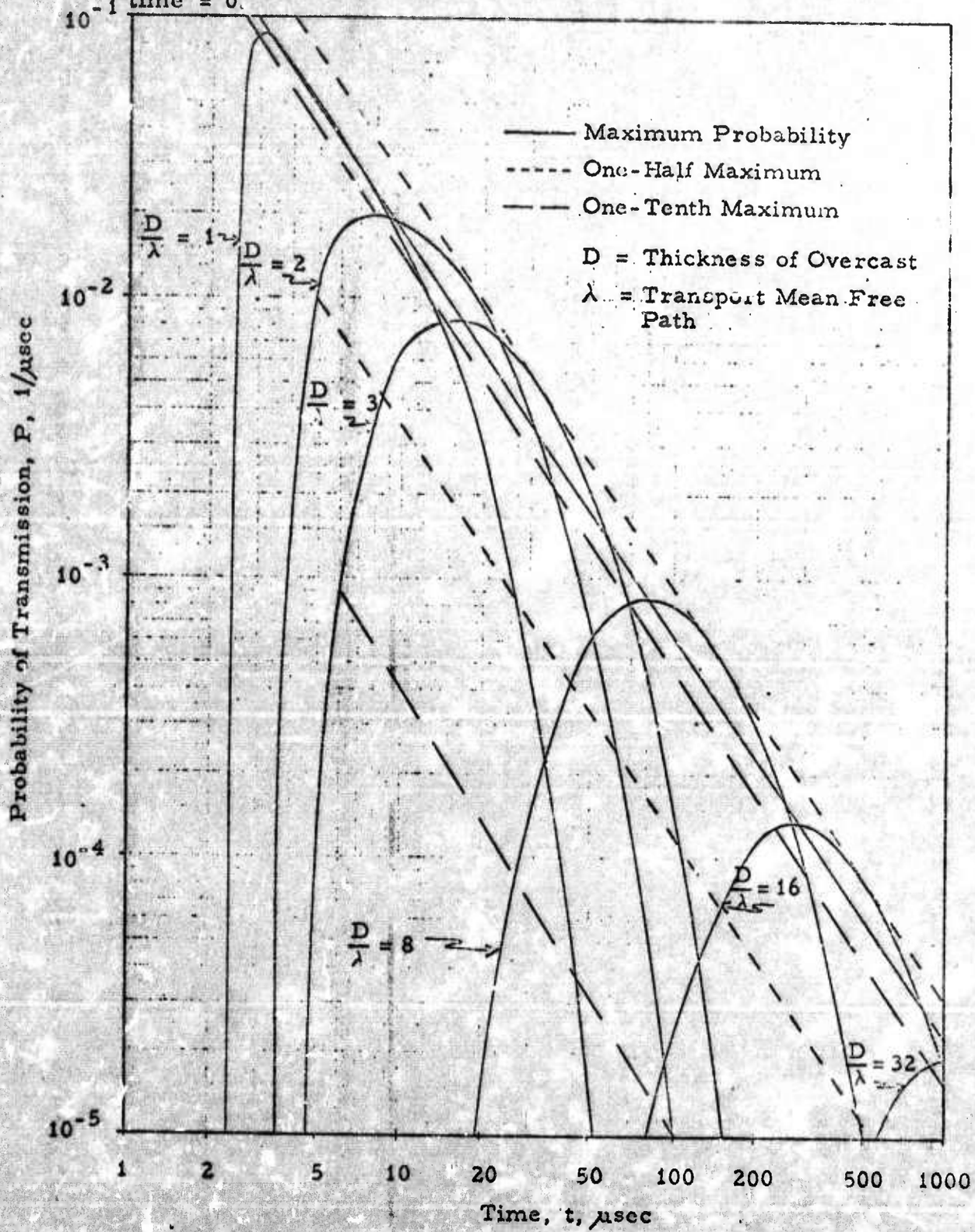

As can be seen in the figure, the shape of the intensity vs. time distribution is the same for clouds where $D >> \lambda$.

The time of the maximum, t_m, in the probability of transmission, is closely given by

$$t_m = .74 \frac{D}{c} \left(\frac{D}{\lambda}\right)^{.7} \tag{4}$$

where

c is the speed of light

A line through the points corresponding to the probability at the time of the maximum is shown in the figure.

An equation for D/λ may be obtained from Equation (3), i.e.,

$$(D/\lambda) = \left[(1-T_{60^\circ})/T_{60^\circ}\right] \tag{5}$$

And the time of the maximum is as follows:

$$t_m = .74 \frac{D}{C} \left(\frac{1-T_{60^\circ}}{T_{60^\circ}}\right)^{.7}$$

Hence, the time of the maximum is a factor greater than one multiplied by the time light takes to penetrate straight through the overcast.

The times at which the probability reaches a given proportion of the maximum value are found to vary as $t^{-3/2}$ for rather thick overcasts, i.e., $D >> \lambda$. Lines corresponding to probabilities of 1/10, 1/2 and equal to the maximum value are shown in the figure and have slope of roughly -3/2. The times at 1/10 maximum value may be expressed in terms of the times at the maximum as

$$t_{1/10} = .37\, t_m \text{ and } 4.4\, t_m$$

and the times at 1/2 maximum value are

$$t_{1/2} = .52\, t_m \text{ and } 2.0\, t_m$$

In the infrared, at wavelengths greater than about 3 microns, the albedoes of the droplets which make up haze and clouds are such that, to a good approximation, thick clouds radiate as black bodies. This does not hold for haze. Table VI shows that the transmission of hazes improves as wavelength increases and thus the thermal emissivity will decrease with increasing wavelength. At 10 microns most hazes are essentially transparent but, at this wavelength, clouds are black. In addition to the emission from water droplets the atmosphere emits in those wavelength regions where the gases of the atmosphere absorb. Figures 3 and 4 show that such emission can occur in the regions between the so-called atmospheric windows. The sky background for day and for night as a function of wavelength is presented in Figures 12 and 13 respectively.

Identification of Figures 12 and 13.

Figure 12:

A - Scattered sunlight, V = 94 km, $\theta = 10^\circ$, $z = 60^\circ$

B - Scattered sunlight, V = 94 km, $\theta = 40^\circ$, $z = 60^\circ$

C - 50% transmitting cloud or fog $\theta = 30^\circ$, $z = 50^\circ$

D - Scattered sunlight, V = 94 km, $\theta = 90^\circ$, $z = 60^\circ$

E - Scattered sunlight, V = 94 km, $\theta = 120^\circ$, $z = 60^\circ$

F - Blackbody at 283° k

G - Emission of water vapor and CO_2

H - Bright Aurora

I - Haze Radiance plus scatter of earth flux:

V = 50 km, $z = 60^\circ$

J - As "I", but V. R. = 94 km

Figure 13:

A - Blackbody at 283° k.

B - Emission of water vapor and CO_2.

C - Bright Aurora

D - Airglow

E - Haze radiance plus scatter of earth flux, $z = 60^\circ$, V = 50 km

F - As "E", but V = 94 km

G - Full moon, V = 94 km, $\theta = 20^\circ$, $z = 60^\circ$

H - Full moon, V = 94 km, $\theta = 90^\circ$, $z = 60^\circ$

I - Full Moon, V = 94 km, $\theta = 40^\circ$, $z = 60^\circ$

J - Maximum scattered city lights

K - Full moon, V = 94 km, $\theta = 10^\circ$, $z = 60^\circ$

θ is the angle through which light is scattered into the viewing path

z is the zenith angle of the viewing path

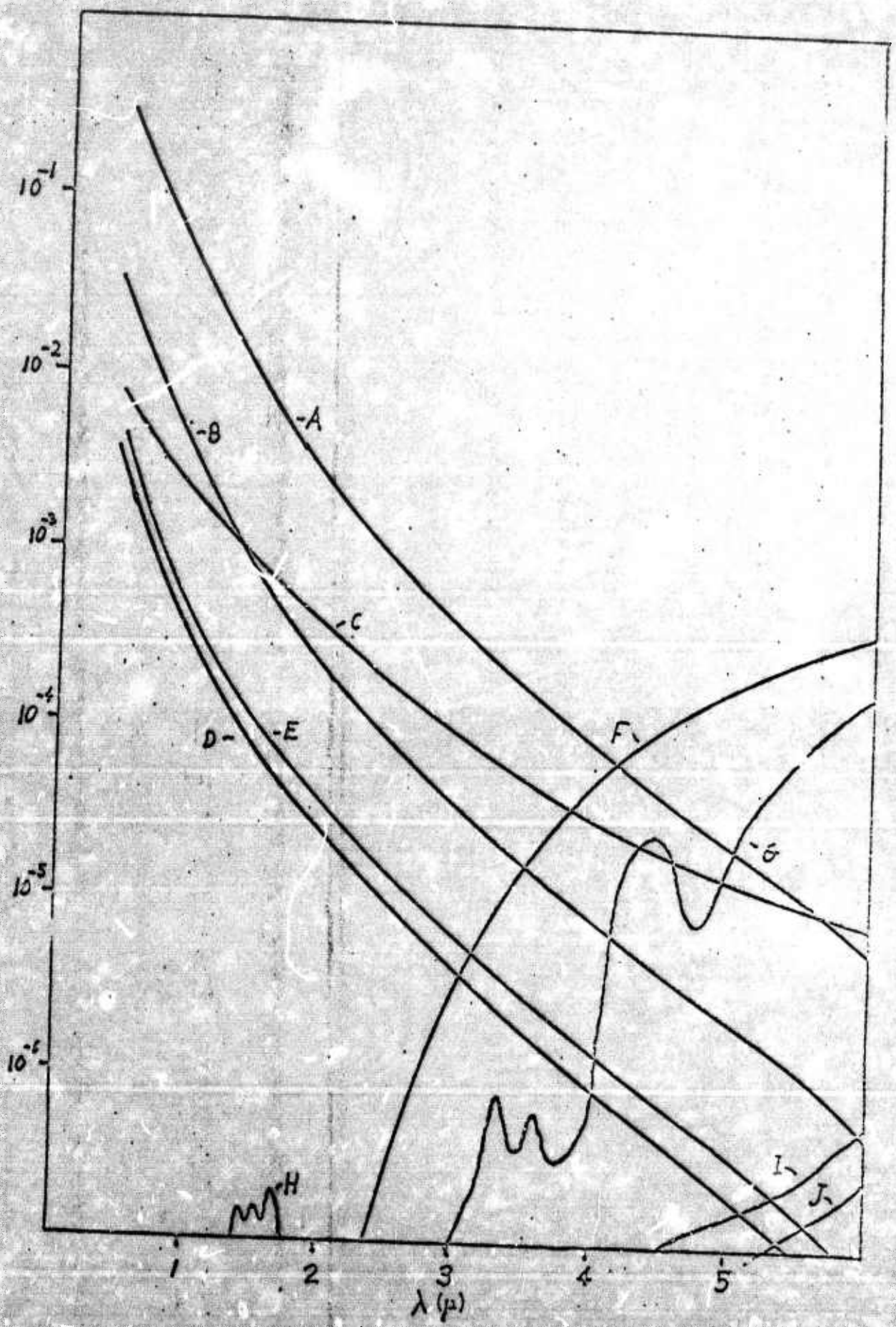
Day Sky Background
Spectral Power Density
(watts, cm^{-2}, μ^{-1}, sr^{-1})
10^{-1}
10^{-2}
10^{-3}
10^{-4}
10^{-5}
10^{-6}
A
B
C
D
E
F
G
H
I
J
1
2
3
4
5
λ (μ)

 Figure 12

Night Sky Background

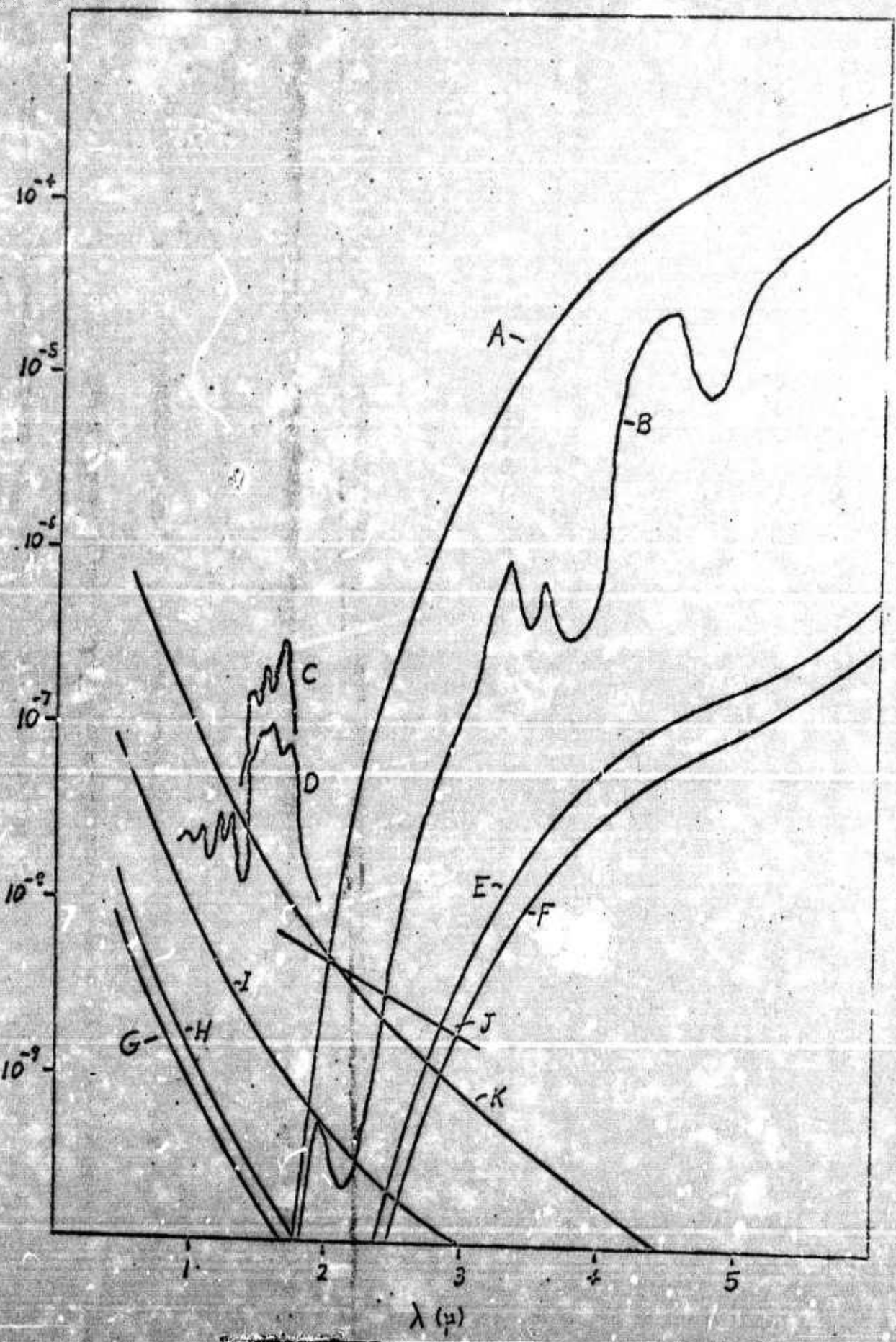

-26- Figure 13

2.5 The Effects of Clouds and Overcast

The effects of clouds and overcast are twofold: First, they may reduce the magnitude of the signal by scattering light from the overcast back into space, and, second, they may distort the signal which would have been received in the absence of the clouds.

Data taken by Eastman Kodak Company from 1937 to date indicate that in Rochester, New York the probability that illumination at the surface of the earth will be cut by clouds to 5 % of clear weather illumination is less than 2.5×10^{-3} and that it will be cut to 10 % is about 10^{-2}.

Probability that there will be some signal reduction and/or distortion due to clouds and overcast have been calculated from United States Department of Commerce, Weather Bureau Paper No. 12, "Sunshine and Cloudiness at Selected Stations, 1951", and from AF Weather Service, Directorate of Climatology, Data Control Division's reports, "Uniform Summary of Surface Weather Observations." The results are given in Table VIII.

Table VIII

Total probability of some signal modification by overcasts or clouds (in per cent)

	Anconge, Alaska	Berlin, Germany	Boston, Massachusetts	Buffalo, New York	Chicago, Illinois	Honolulu, Hawaii	Paris, France	Rochester, New York	Sacramento, California	Washington, D. C.	Yuma, Arizona
Jan	71	75	58	79	63	52	59	72	57	59	24
Feb	74	72	54	72	61	51	85	67	43	55	24
Mar	69	60	56	67	60	57	69	61	42	55	21
Apr	70	60	56	61	57	54	13	51	35	52	15
May	75	60	56	58	53	51	61	54	27	52	10
Jun	71	64	55	53	51	50	73	45	17	50	6
Jul	76	61	55	50	42	48	48	48	7	50	16
Aug	70	61	51	51	43	13	68	49	8	50	13
Sep	74	56	50	53	47	49	56	58	14	47	11
Oct	78	62	52	62	50	51	58	63	24	45	12
Nov	70	79	57	76	62	55	72	81	37	53	17
Dec	71	78	58	81	65	54	64	87	56	58	21
Annual	73	66	55	64	54	52	64	62	31	52	16.3

2.51 Cloud Characteristics

The following information about cloud characteristics was taken from the "Handbook of Meteorology by Berry, Bollay, and Beers, McGraw-Hill (1945):

Clouds are divided into four families with reference to height above the ground level in the region.

Family A	High clouds (mean lower level 6 km)
Family B	Middle clouds (mean upper level 6 km, mean lower level 2 km)
Family C	Low clouds (mean upper level 2 km, mean lower level close to the ground)
Family D	Clouds with vertical development (mean upper level that of cirrus, mean lower level .5 km)

At nearly all levels, clouds may appear under the following forms:

a. Isolated heap clouds with vertical development during their formation, and a spreading out when they are dissolving.

b. Sheet clouds, which are divided into filaments, scales, or rounded masses, and which are often stable or in process of disintegration.

c. More or less continuous cloud sheets, often in process of formation or growth.

The following table indicates the cloud genera, with the observed form of each:

Family	Genus	Form		
		a	b	c
A	Cirrus		x	
	Cirrocumulus		x	
	Cirrostratus			x
B	Altocumulus	x	x	
	Altostratus			x
C	Stratocumulus	x	x	
	Stratus			x
	Nimbostratus			x
D	Cumulus	x		
	Cumulonimbus	x		

2.6 Noise in the Sky

Under ideal conditions and with a perfect radiation detector, the noise in a signal or the noise from a background can be calculated on the basis of statistical fluctuations in the number of photons reaching the detector. This situation almost never occurs in atmospheric work. Noise in the signal arises from scintillation and seeing problems, and noise in the background level is generated by space and time variations in the scattering or emitting media responsible for background signals. Particular interest in the background noise seen by systems which scan the sky has resulted in studies of sky noise as a function of scanning rate. Resulting data are usually summarized in a presentation known as a Wiener Spectrum.[12] Four typical Wiener Spectra for a circular scan are shown in Figure 14.

Turbulence in the atmosphere, particularly in the tropopause causes spatial and time variations in refractive index. One may think of this effect as producing refractive cells having dimensions of the class of three to eight inches. Cells deviate the light passing through them causing variations in the position of the stellar image in a telescope (seeing) and also fluctuating shadows on the aperture of the telescope (scintillation). The lifetime of the cells is of the order of 0.05 seconds and they may move with the winds aloft (velocity up to 120 mph).

For observatories on the earth's surface astronomical resolution is limited by the seeing described above to approximately 3×10^{-6} radians. In general, daytime resolution does not exceed 1 or 2×10^{-5} radians for a vertical path. Approximate calculations can be made for camera systems looking down through the atmosphere using the equation $\Delta x = \alpha_{(z)} h$, where Δx = minimum resolvable distance on ground, measured perpendicular to sight path, $\alpha_{(z)}$ = mean deviation angle of light passing through scintillation layer at zenith angle z, and h = distance from ground to scintillation layer.

Figure 14 (from ref. 12)

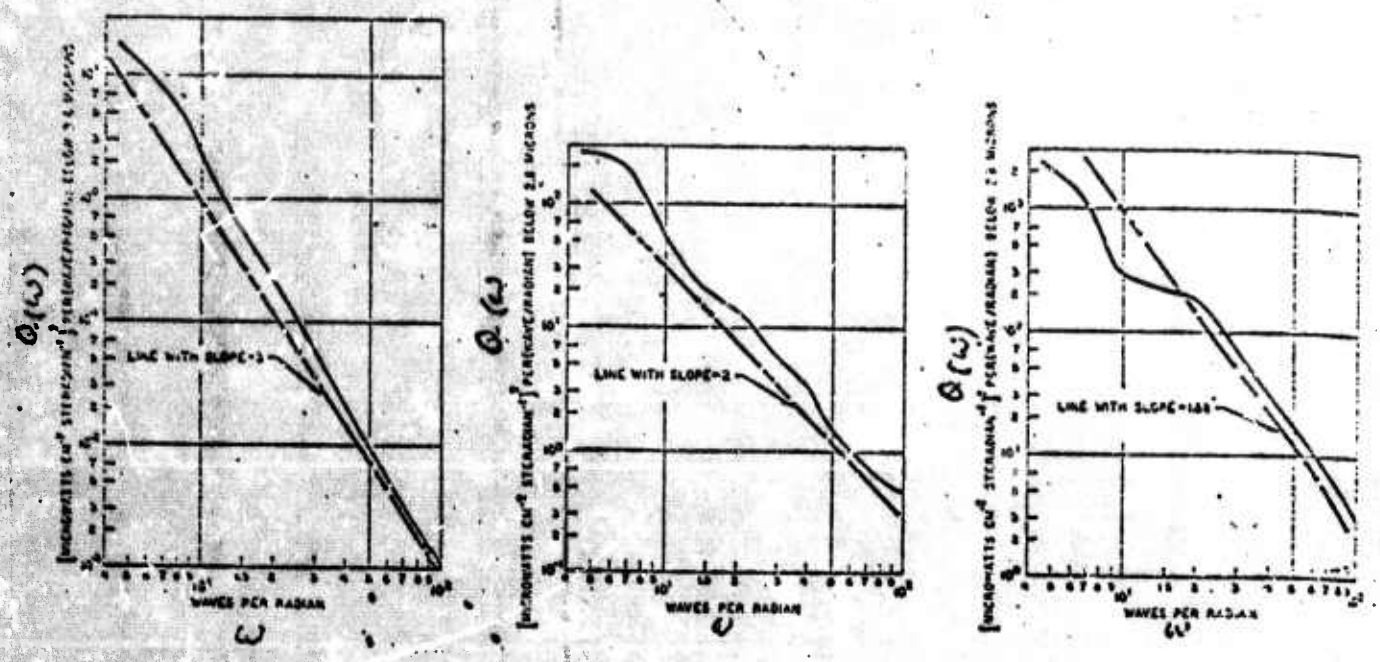

For scanners with a small instantaneous field of view Ω (sr), the noise power input N (μ watts) to a detector viewing aperture A (cm^2) is

$$N = A\,\Omega \left[\int_{f_1/s}^{f_2/s} Q(\omega)\, d(\omega)\right]^{1/2}$$

where s is scan rate (rad/sec), $f_1 \rightarrow f_2$ is the time frequency band-pass of the system, ω is spatial frequency (cpr) and Q is the function plotted above. This evaluation is accurate only when the largest angular dimension of the field is less than f_1/s. More complex geometries are treated in the literature.

2.61 Atmospheric Scintillation

Calculations of the scintillation of an extended source are reported in Appendix B. A summary of these results will be presented here.

One may understand the calculated results by means of the following model: The refractive cells move as they decay across the projection of the telescope onto the turbulent layer. Since most scintillation occurs near the tropopause, we take the height of the turbulent layer as the height of the tropopause, about 10 km at middle latitudes. There are various sizes of refractive cells, and which ones contribute the most to scintillation must be determined. The geometry is shown in Figure 15.

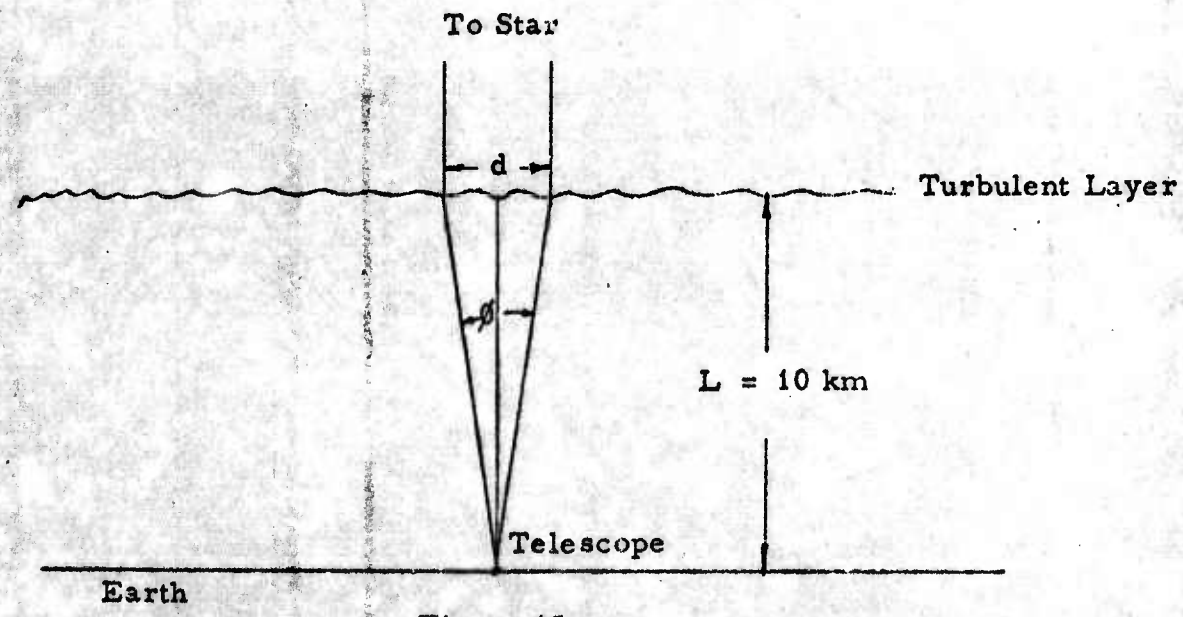

Figure 15

Consider a turbulent cell of diameter d. Its diffraction pattern on the ground has an angular width θ of about $\theta \simeq \lambda/d$, where

λ is the wave length of light. The angular extent of the cell at the telescope, ϕ, is given by $\phi = d/L$, where L is the height of the turbulent layer. The geometrical shadow of the cell will be equal to the diffraction pattern of the cell when $\theta = \phi$. For smaller cells, i.e., $\theta > \phi$, the geometrical shadow essentially disappears. For larger cells, i.e. $\theta < \phi$, the cell population is much less than for the smaller cells. The diameter of the cell for which $\theta = \phi$ is $d_o = \sqrt{\lambda L}$. Hence, cells of about diameter $d = d_o$, will mainly affect scintillation. As a result, the scintillation of a star as received by a point detector could be considered as having come through a cell of diameter $d = d_o = \sqrt{\lambda L}$. The length $d_o/2$ is the correlation length on the ground for two detectors, by a similar argument. An extended source, therefore, may be considered as being made up of cells of length d_o. The scintillation noise from each cell is uncorrelated. Those cells which are not on the edge of the source, i.e., internal cells, give no contribution to the scintillation, due to the fact that light scatters from one internal cell to another. An extended source projected onto the turbulent layer is shown in Figure 16 below.

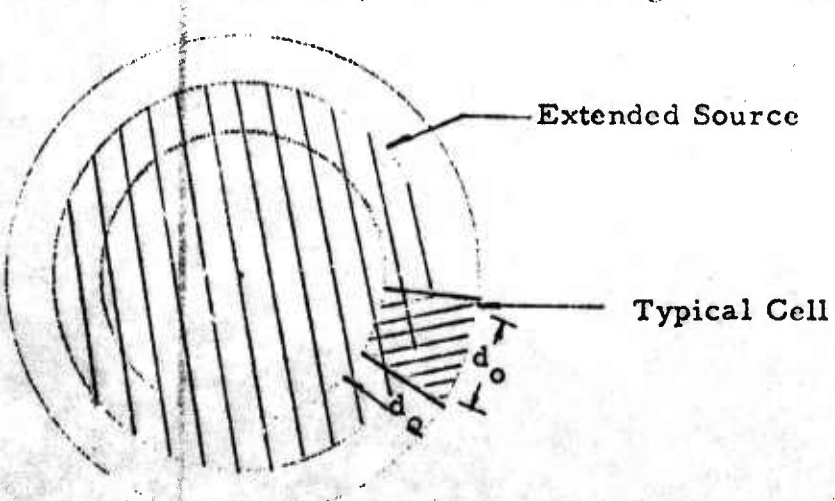

Figure 16

The edge of the source is broken up into cells, each of size d_o, twice the correlation length. Since the scintillation contribution from each cell is incoherent, the total contribution is given by multiplying the scintillation noise by the square root of the number of cells. However, the source in each cell is coherent, so the total source is given by multiplying the source in each cell by the number of cells. Hence, if the scintillation noise-to-signal noise ratio is measured for a star, one can calculate very closely, using the equation given below, the noise-to-signal ratio of the sun, as measured by the same instrument.

$$(n/s)_{sun} = k(n/s)_{star} (\sqrt{N_s}/N_s)(A_r/A_s) \qquad (6)$$

where

$(n/s)_{sun}$ = Noise-to-signal ratio of the sun,

N_s = Number of correlation cells on the circumference of the sun,

A_r = Source area of ring of correlation cells,

A_s = Sun area,

k is a constant which accounts for the adjacent correlation cells on the sun.

The geometry is illustrated in Figure 17 below:

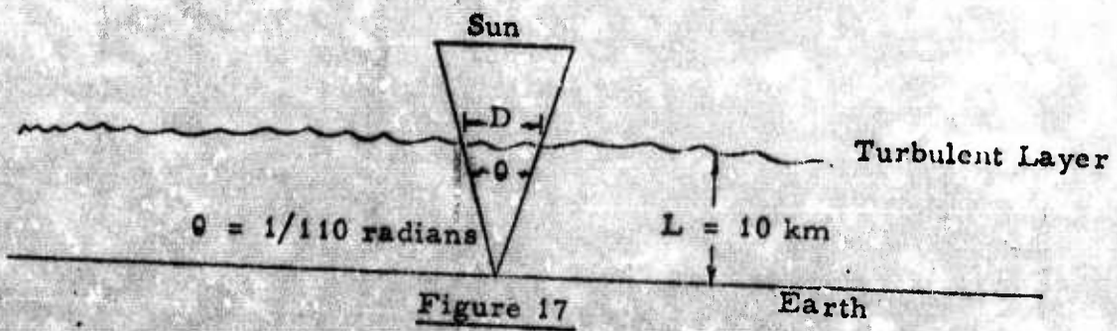

Figure 17

For purposes of the present discussion we may consider the cells as squares on the edge of the sun. Now the number of correlation cells on the circumference of the sun is

$$N_s = \pi D/d_o$$

And

$$A_r = \pi D(d_o/2)$$

$$A_s = \pi D^2/4$$

Therefore,

$$A_r/A_s = 2d_o/D$$

And $(n/s)_{sun}$ becomes

$$(n/s)_{sun} = k(n/s)_{star}\,(2/\sqrt{\pi})(d_o/D)^{3/2} \qquad (7)$$

To calculate k, one may observe that roughly half of the scintillation noise from a given cell will fall on one of the two adjacent edge cells, and should therefore not be counted as noise. This indicates that $k \simeq 1/2$. A more exact calculation shows that

$$k = \left[\sqrt{(n/s)_{star} + 1} - 1\right](s/n)_{star} \qquad (8)$$

Since $(n/s)_{star} \leq 1$, Equation (8) gives $k \simeq 1/2$. Now, the cell size d_o, is equal to $(\lambda L)^{1/2}$, and the diameter of the sun projected on the turbulent layer is $D = \theta L$. Substituting all these relations into Equation (6) gives

$$(n/s)_{sun} = \left[\sqrt{(n/s)_{star} + 1} - 1\right] (2/\sqrt{\pi})(110)^{3/2}(\lambda/L)^{3/4} \quad (9)$$

The measured value of $(n/s)_{star}$ is approximately 1 for an instrument whose aperture is less than the area of a correlation cell, roughly $A_c \simeq (d_o/2)^2 \simeq 13\ cm^2$. With this value and with $\lambda \simeq 5000$ Å, Equation (9) becomes

$$(n/s)_{sun} \simeq 1.0 \times 10^{-5}$$

A more exact calculation, given in Appendix B, yields 9.42×10^{-6}.

The stellar scintillation decreases as the radius of the telescope, for telescopes of larger diameter than the correlation length. This fact may be understood by noting that the telescope may be broken up into correlation areas. The contribution of each area is incoherent, whereas the source is coherent. Hence, the total scintillation noise-to-signal ratio is inversely proportional to the square root of the number of correlation areas within the telescope aperture. This is the same as to the scintillation noise-to-signal ratio, varying inversely with the radius of the telescope.

2.62 Frequency Spectrum of Scintillation

The frequency spectrum of scintillation is dependent upon the aperture of the telescope used, the size distribution of the refracting cells, their lifetime, their height and their velocity of motion. Figure 18, a, b and c, presents characteristic results of scintillation studies. For resolution of the class of 3×10^{-6} radians, seeing and scintillation are independent of zenith angle if $z < 60^\circ$. For poor

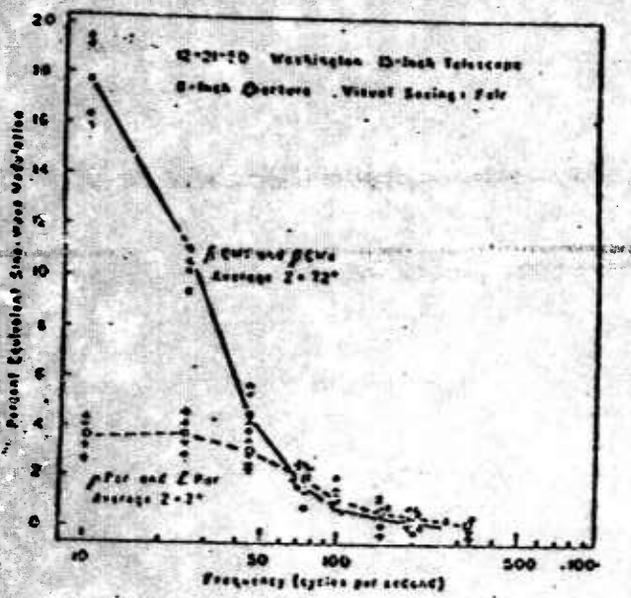

FIG. 5. Scintillation spectra, showing the increase of scintillation with zenith distance.

a

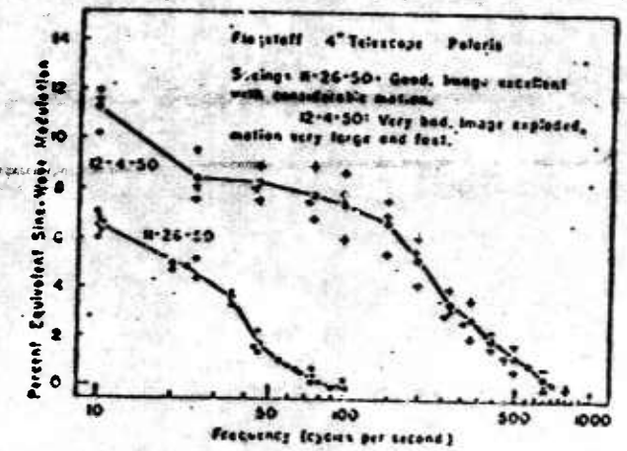

FIG. 4. Scintillation spectra with good and bad visual seeing at the Lowell Observatory, Flagstaff, Arizona. Surface winds were from north to northeast on both dates, barely perceptible on 11-26-50, but breezy on 12-4-50.

b

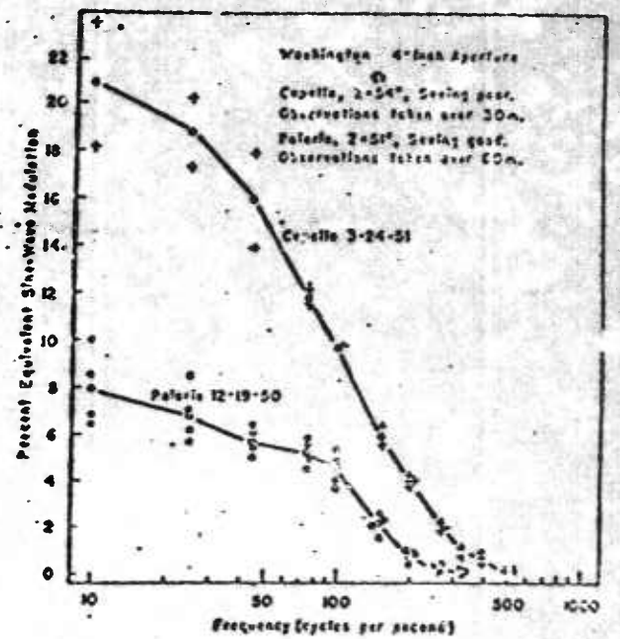

FIG. 3. Scintillation spectra observed at Washington under widely different conditions of visual seeing. Both nights were calm. Open circles indicate means of the observational points.

c

Figure 18 (from ref. 13)

resolution (less than 10^{-5} radians) the variation is approximately $(\sec z)^{1/2}$, and the amplitude of scintillation increases roughly in the same manner.

The scintillation frequency spectrum results from the scintillation of turbulent cells of different sizes. These cells move at wind velocity and decay with a lifetime of roughly .05 sec, as was mentioned above. Hence, for any source of reasonable size, the turbulent cells move across it before they decay. As a result, each frequency in the scintillation spectrum is due to a cell of different size, with the larger cells giving lower frequencies.

The experimental data given in Appendix E indicates that the frequency spectrum for an extended source, in this case the sun, is roughly the same as that for a point source like a star, except that lower frequencies give relatively more scintillation than the higher ones for the case of an extended source. This may be understood in the following way: In Equation (7) the scintillation noise-to-signal ratio for an extended source is shown to be proportional to the noise-to-signal ratio for a point source multiplied by the ratio of the size of a turbulent cell to the projected diameter of the source, to the 3/2 power. There, the cell used was interpreted as the average cell. Now, since each cell size contributes to a different frequency in the scintillation power spectra, Equation (7) may be interpreted as the frequency-dependent noise-to-signal ratio of the point source and extended source. It then predicts that the scintillation as a function of frequency for an extended source has a faster variation with frequency than for a point source, which seems to match the data obtained and reported in Appendix E.

REFERENCES

1. H. Stewart and R. Hopfield, "Atmospheric Effects," EHPA Report No. 55683, May 6, 1963.

2. M. Basilio, D. Fox, H. Stewart, Final Report on the Distortion of Pulsed Light Signals by Scattering in and Between Clouds, Contract AF(29-1)-1183, Subcontract (113-2), July, 1961.

3. C. W. Allen, Astrophysical Quantities, Chap. 6, The Athlone Press, London, 1955.

4. A. I. Mahan, "Astronomical Refraction, Some History and Theories," Applied Optics, 1, 497-511, July, 1962.

5. Handbook of Geophysics, Revised Edition, Chap. 8, MacMillan, New York, 1960.

6. Modified from W. E. K. Middleton, Vision Through the Atmosphere, p. 45, Univ. of Toronto Press, Toronto, 1958.

7. H. C. Van de Hulst, Light Scattering by Small Particles, Part II, p. 65, Wiley, New York, 1957.

8. D. Deirmendjian, "Scattering and Polarization Properties of Polydispersed Suspensions with Partial Absorption," p. 9, Rand Corporation Memorandum RM-3228-PR, 1962.

9. Effects of Night Sky Backgrounds on Optical Measurements, "pp. 25, 26, Geophysics Corp. of America, March 6, 1959.

10. S. K. Mitra, The Upper Atmosphere, p. 486, Asiatic Society, Calcutta, 1952.

11. H. C. Van de Hulst in The Atmosphere of the Earth and Planets, Chap. 3 (G. P. Kuiper, Ed.), Univ. of Chicago Press (194 ?).

12. G. F. Aroyan, "The Technique of Spatial Filtering," Proc. Inst. Radio Engineers, 47, p. 1564, 1959.

13. A. H. Mikesell, A. A. Hoag and J. S. Hall, "The Scintillation of Starlight," J. Opt. Soc. Amer., 41, pp. 691, 692, 1951.

APPENDIX A

Resonant Scattering and Excitation Transfer for the Lyman-Birge-Hopfield Series and for the First Positive System of Nitrogen

by E. Zipf

I. Excitation of the Lyman-Birge-Hopfield Sytem of Nitrogen by Resonance Scattering

The Lyman-Birge-Hopfield system of nitrogen (LBH) is a conspicuous feature in the ultraviolet auroral spectrum. The system is emitted by nitrogen molecules in a radiative transition from the $a^1\pi_g$ state to the ground state $X^1\Sigma^+_g$. Electric dipole transitions from the $a^1\pi_g$ state to the ground state are forbidden by the symmetry selection rule $g \not\rightarrow g$ so that the $a^1\pi_g$ state is metastable.

For the most part the brightest bands of the Lyman-Birge-Hopfield system are emitted in the wavelength region 1100Å-2000Å; strong absorption by O_2 at these wavelengths precludes any possibility of observing these bands from the ground. In auroras the LBH system appears to be excited by electron bombardment as well as by cascade radiation from higher singlet states. Presumably these processes would also lead to the emission of the LBH bands following an atomic bomb explosion. In this connection, however, the following question can be raised: Does resonance scattering of ultraviolet photons from the explosion by ground state nitrogen molecules contribute in a significant way to the emission of the Lyman-Birge-Hopfield system?

The photon emission rate per second per N_2 molecule in the v'-v'' band of the LBH system due to resonance scattering by $N_2(X^1\Sigma^+_g)$ molecules in the v'' = 0 level is given by

$$g = \pi F_{av} \frac{\pi e^2}{mc} f_{o,v'} \frac{A_{v',v''}}{\sum_{v''} A_{v',v''}} \qquad (1)$$

where $f_{o,v'}$ is the f-value for absorption from $v'' = 0$ to v' in the upper state and F_{av} is the incident flux of photons per unit frequency interval per unit time per unit area (Chamberlain, 1961). The oscillator strength $f_{v',v''}$ is related to the transition probability $A_{v',v''}$ by

$$f_{v',v''} = 1.5 \times 10^{-8} \lambda^2_{v',v''} A_{v',v''}$$

and

$$(1/\tau_{v'}) = \sum_{v''} A_{v',v''} \qquad (3)$$

$\tau_{v'}$ is the radiative lifetime of the vibrational level v'. Lichten (1957) has obtained an approximate value of 1.7×10^{-4} sec for $\tau(a'\pi_g)$.

Given the minimum signal detectable by a satellite LBH-photometer one can determine from Equation (1) (making allowance for absorption by O_2) what class of bombs can provide the required flux for an observable signal. The prospects for a workable detection system based on the excitation of the LBH system by resonance scattering alone are not very good because the comparatively long lifetime of the $a^1\pi_g$ state results in a low scattering efficiency. A useful rule of thumb may be derived from the recent dayglow experiments of Fastie et al. (1964), who found that under normal conditions (no auroral activity) there is no observable LBH emission (<100 rayleighs) in the dayglow. This would imply that the flux incident on the upper atmosphere in the 1100Å-2000Å region of the spectrum from a bomb explosion would have to be considerably more intense than the solar flux at these same wave lengths to produce a detectable effect.

II. Excitation of the First Positive System of Nitrogen by Collisions of the Second Kind with Metastable Nitrogen Molecules in the $a^1\pi_g$ State

Oldenberg (1959) has advanced the hypothesis that the reaction

$$N_2(a'\pi_g) + N_2 \longrightarrow N_2(B^3\pi_g) + N_2 \qquad (4)$$

is the principal excitation mechanism for the First Positive bands of nitrogen in the Thompson-Williams (1934) afterglow. This afterglow is produced by bombarding N_2 at a pressure of 3×10^{-3} mm Hg with electrons at energies greater than 10 ev. The experimental data are in qualitative agreement with Oldenberg's theory. However, no estimates are available of the magnitude of the cross section for process (4). More experimental work is desirable.

REFERENCES

Chamberlain, J. W., Physics of the Aurora and Airglow, Academic Press, New York, 1961.

Lichten, W., J. Chem. Phys. 26, 306 (1957).

Oldenberg, O., Planet. Space Sci. 1, 40 (1959).

Thompson and Williams, Proc. Roy. Soc. A147, 583 (1934).

Fastie, W., H. M. Crosswhite, and D. F. Heath, Rocket Spectrophotometer Airglow Measurements in the Far Ultraviolet, Report No. 5, N. A. S. A. Grant NsG 193-62, Johns Hopkins University, Baltimore, 1964.

APPENDIX B

The Effects of Overcasts on the Light Received by the VELA System

by J. DeGroot

This appendix has been abstracted from a series of reports prepared at E. H. Plesset Associates under AFTAC Contract No. AF 33(657)-13599. These reports discuss the effects of clouds and overcasts on the signature of X-ray induced fluorescent light received by the VELA system. The source of the X-rays is a nuclear burst in space. Specifically, the results of this work are presented in the form of curves of the intensity of light received by a VELA detector with an overcast present relative to the intensity recieved without an overcast. The nuclear burst is assumed to occur at the zenith of the detector and far enough away so that the X-ray pulse is a plane wave when it strikes the fluorescent layer. The fluorescent layer is assumed to be optically thin, and the fluorescence is assumed to occur in a very thin layer at an altitude of 80 km.

With these assumptions for the source of light, a uniform overcast, infinite in two directions, was used in the calculations. The geometry is shown in Figure 1 below:

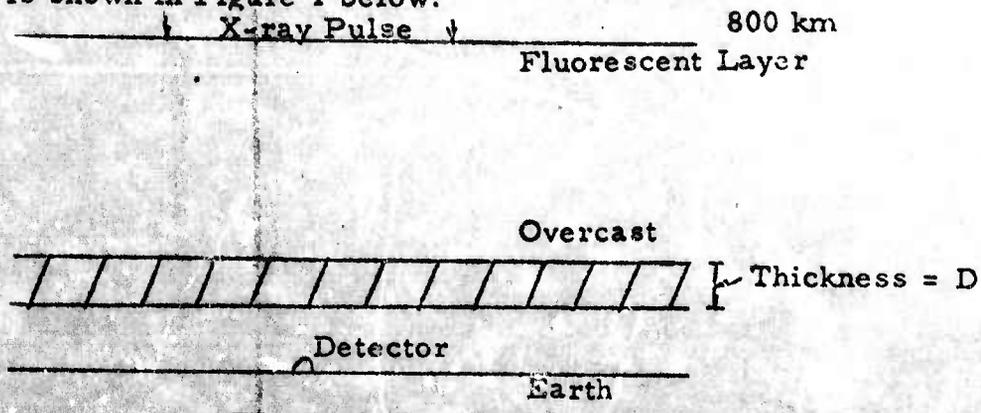

Figure 1

The time dependent transmission of the overcast was calculated using diffusion theory. The detector was assumed to have an isotropic response out to 80° from the vertical.

The calculations were done on an IBM 1620 binary digital computer. Overcast thickness, height, and diffuse transmission were parameters. Calculations were made with overcast thicknesses of 1 km, 2 km, 4 km, and 6 km, and with overcast heights of 1 km, 2 km, 4 km. and 6 km. Overcast diffuse transmissions which were used are: .07, .15, .25, .35, and .50 .

The resulting set of curves are shown in Figures 2-11. For each curve, the relative intensity received by the VELA system is shown without clouds as a function of time. The origin in time is when the first light is received at the detector. The curves are normalized to the light intensity received without an overcast at the origin in time. The overcast thickness and height are constant on each figure, while the overcast diffuse transmission is varied.

One effect that can be seen in all the figures is that the overcast can sharpen the light pulse. This occurs for a thin overcast, i.e., $T_{60^{\circ}} \simeq .5$. The physical reason for this is that the overcast acts only to redirect, not to diffuse, light. Hence, the overcast may be considered to be a flat detector, which has an extra cosine factor in the light intensity received over that received without clouds.

Figure 2

Relative Fluorescent Light Intensity vs. Time

For an Overcast of Various Diffuse Transmissions

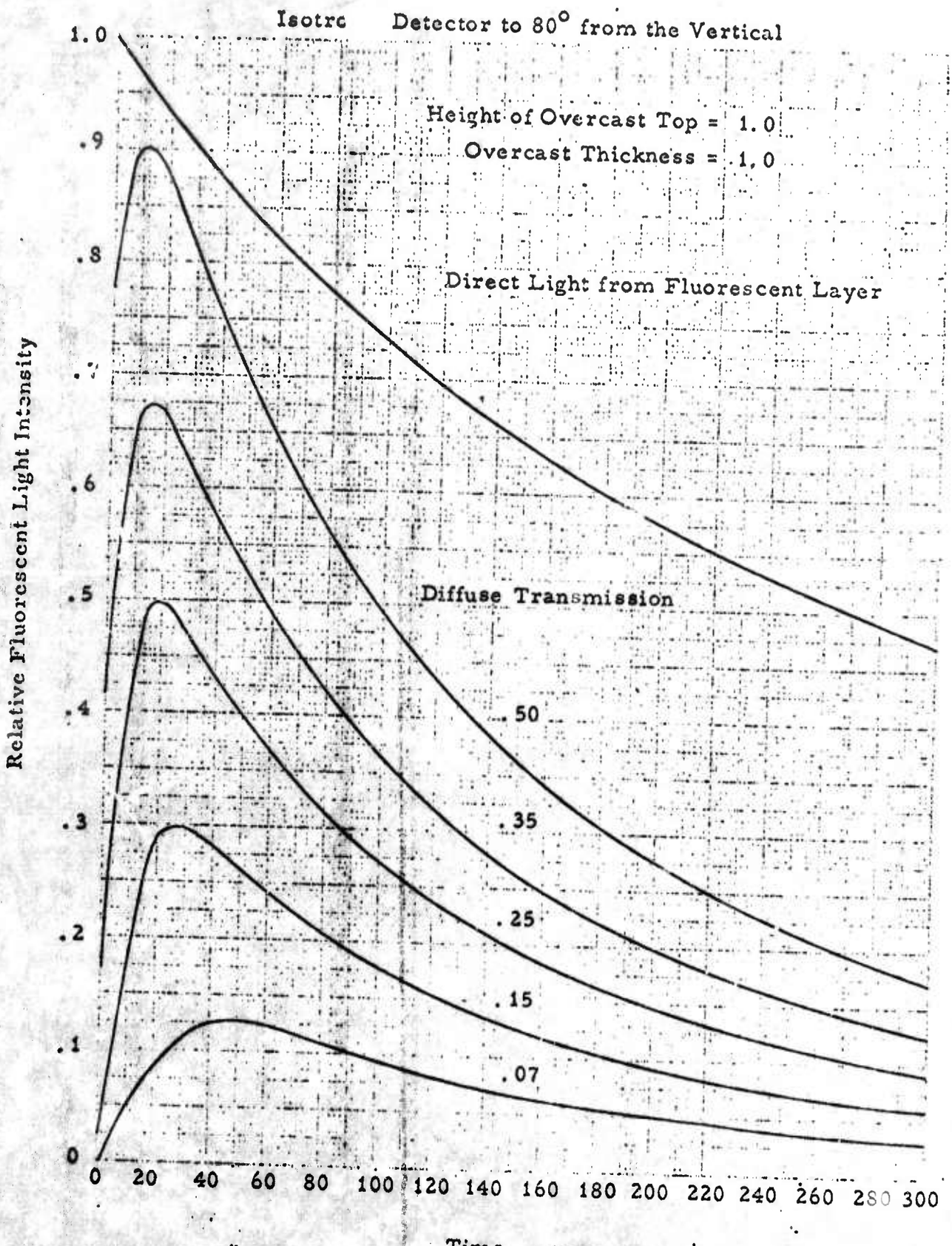

Figure 3

Relative Fluorescent Light Intensity vs. Time

For an Overcast of Various Diffuse Transmissions

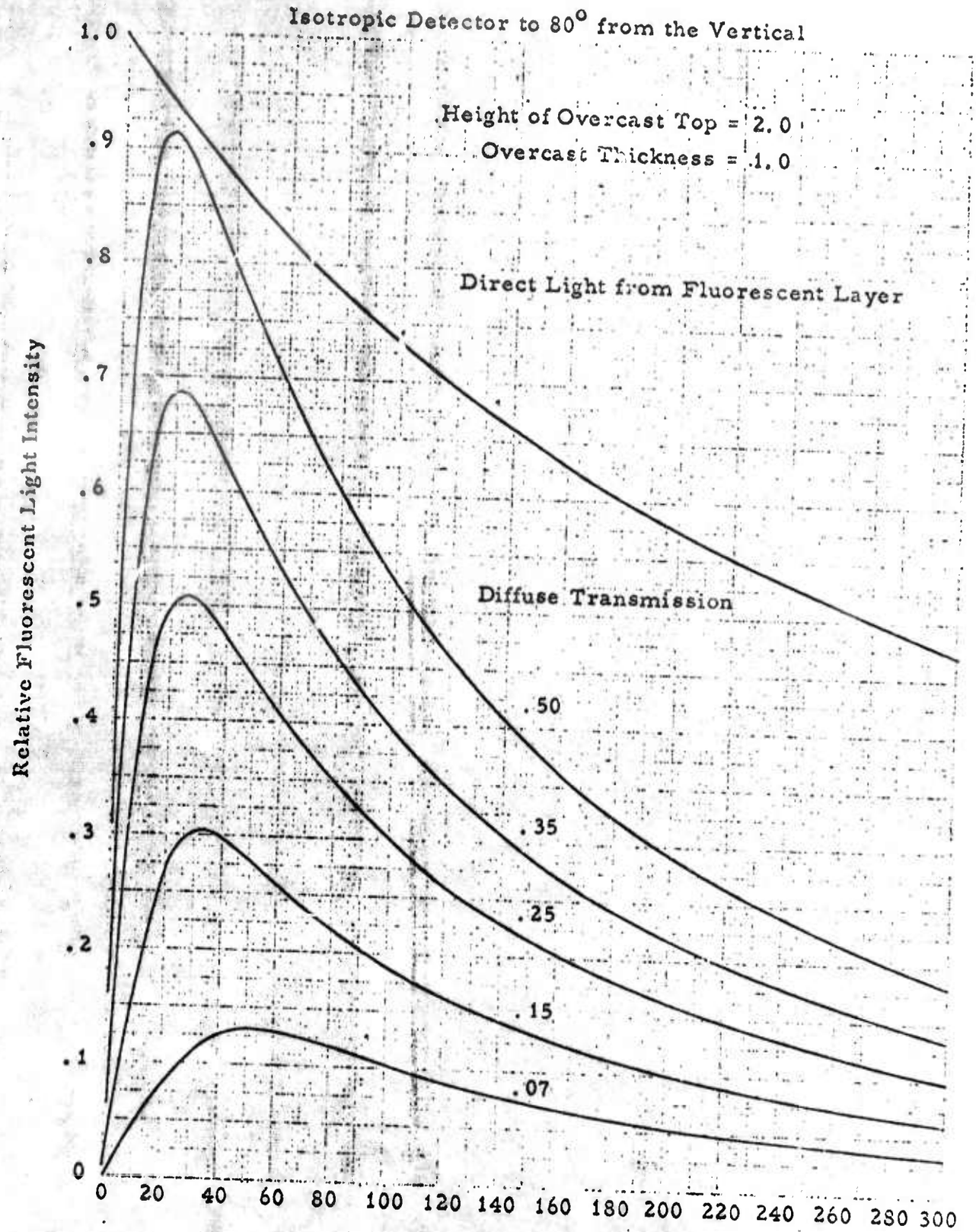

Figure 4

Relative Fluorescent Light Intensity vs. Time

For an Overcast of Various Diffuse Transmissions

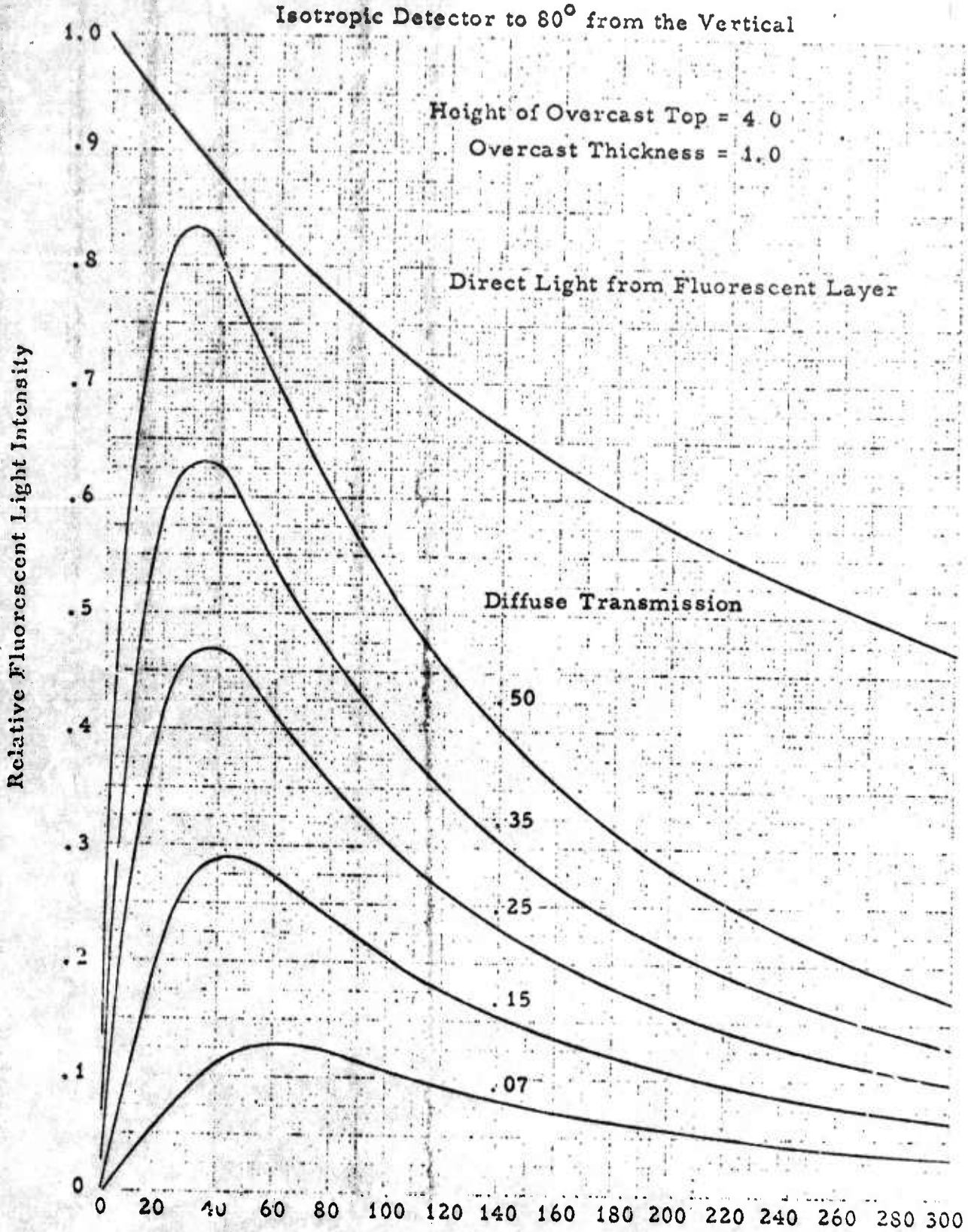

Figure 5

Relative Fluorescent Light Intensity vs. Time

For an Overcast of Various Diffuse Transmissions

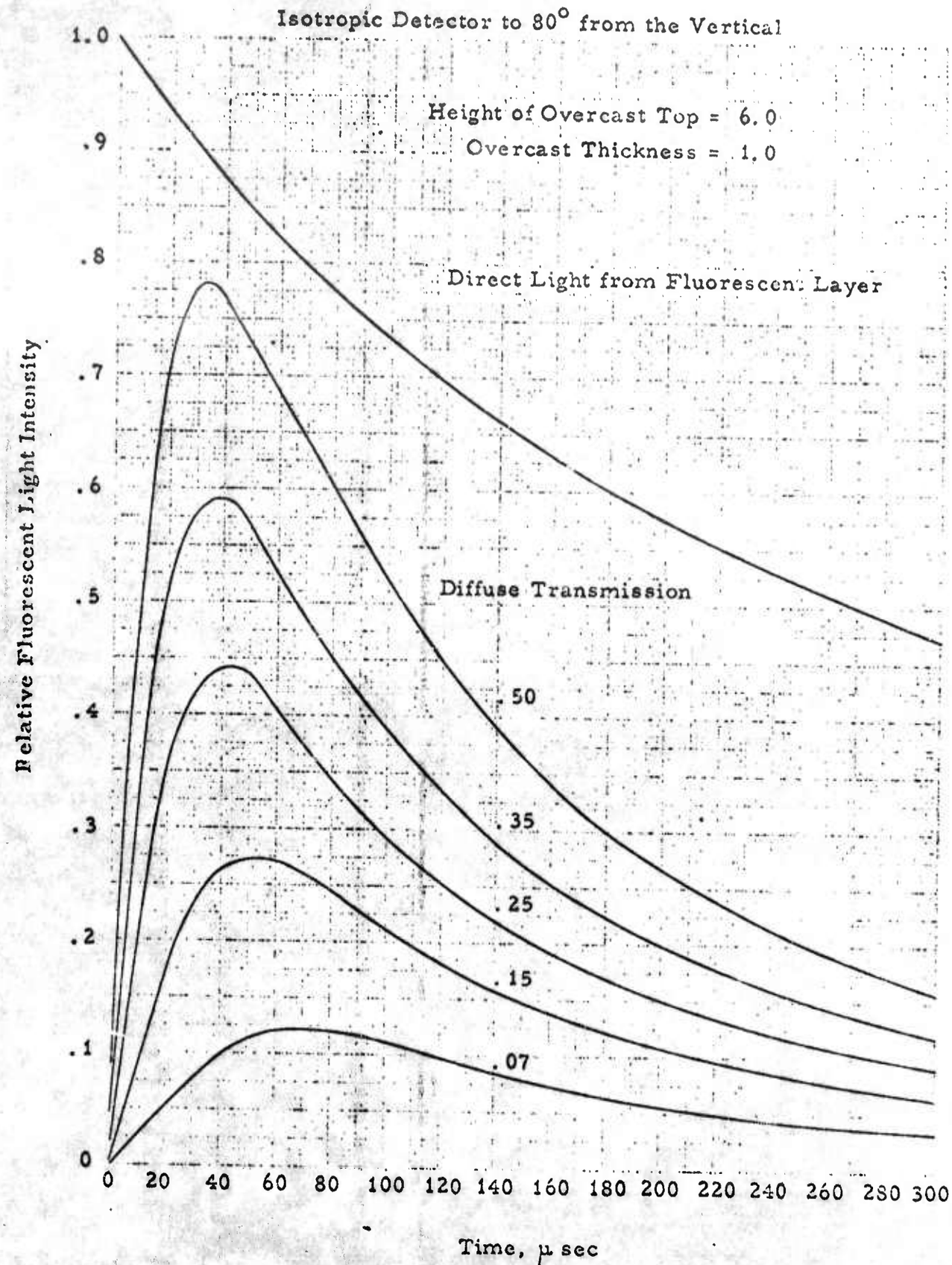

Figure 6

Relative Fluorescent Light Intensity vs. Time
For an Overcast of Various Diffuse Transmissions

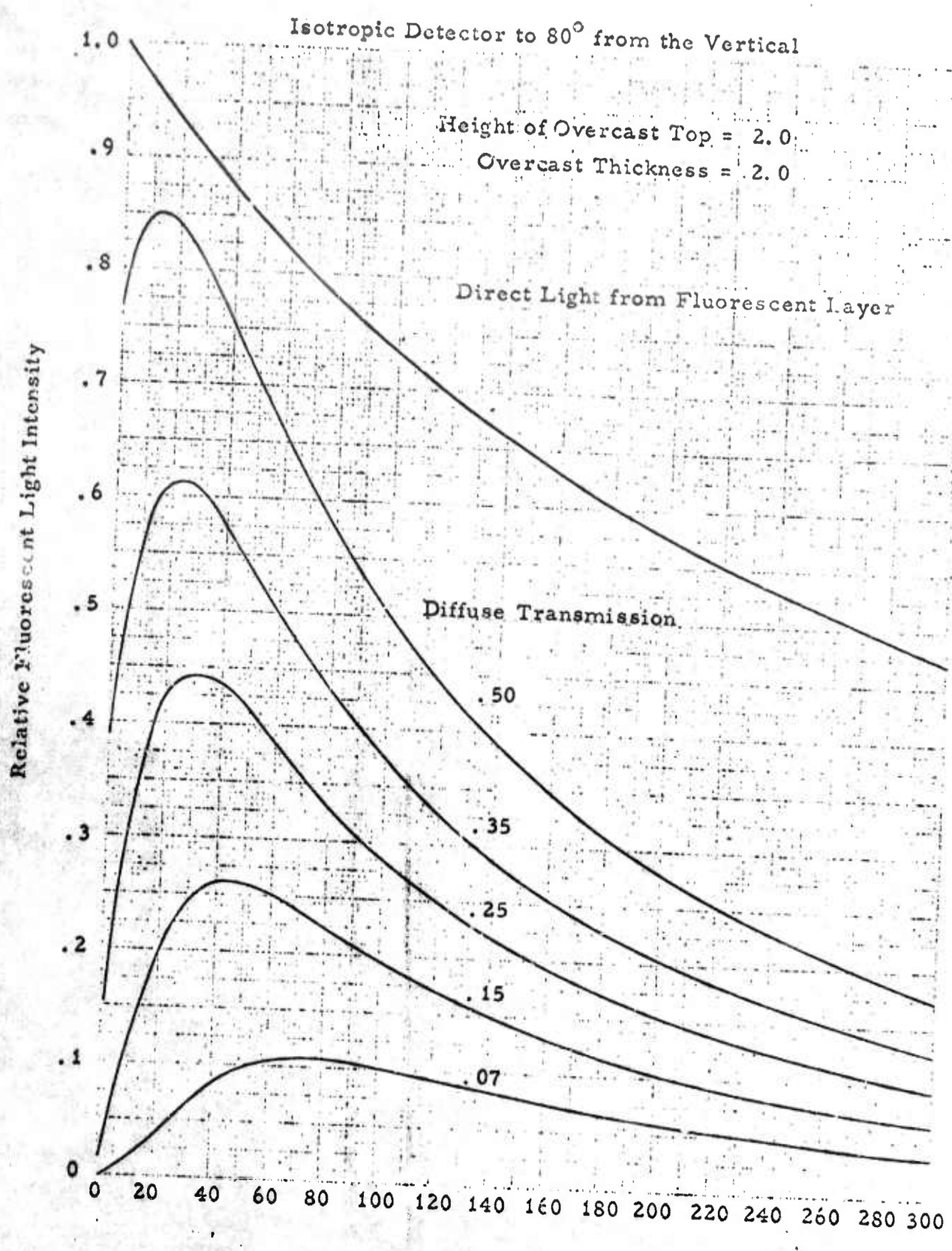

Figure 7

Relative Fluorescent Light Intensity vs. Time

For an Overcast of Various Diffuse Transmissions

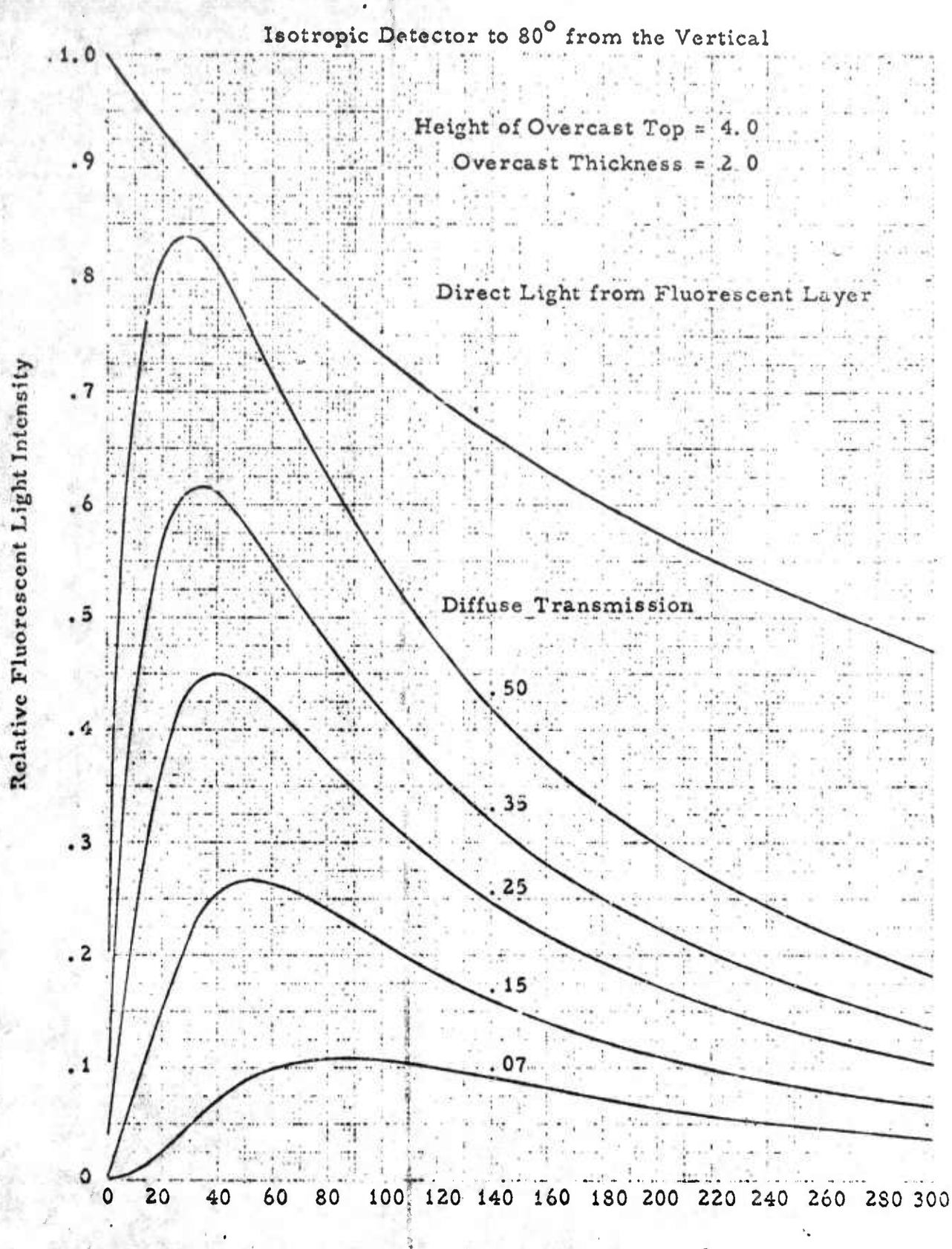

Figure 8

Relative Fluorescent Light Intensity vs. Time

For an Overcast of Various Diffuse Transmissions

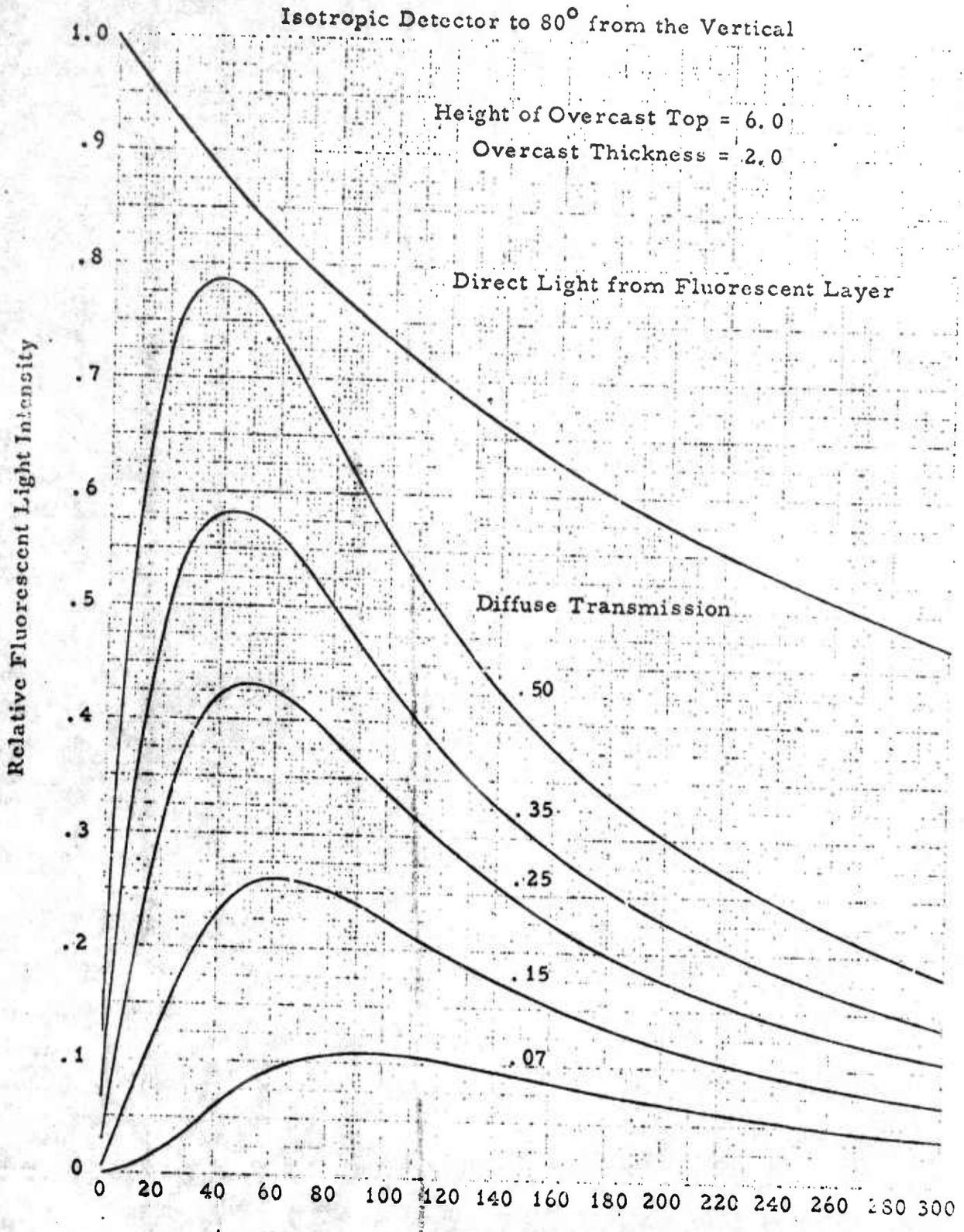

Figure 9

Relative Fluorescent Light Intensity vs. Time

For an Overcast of Various Diffuse Transmissions

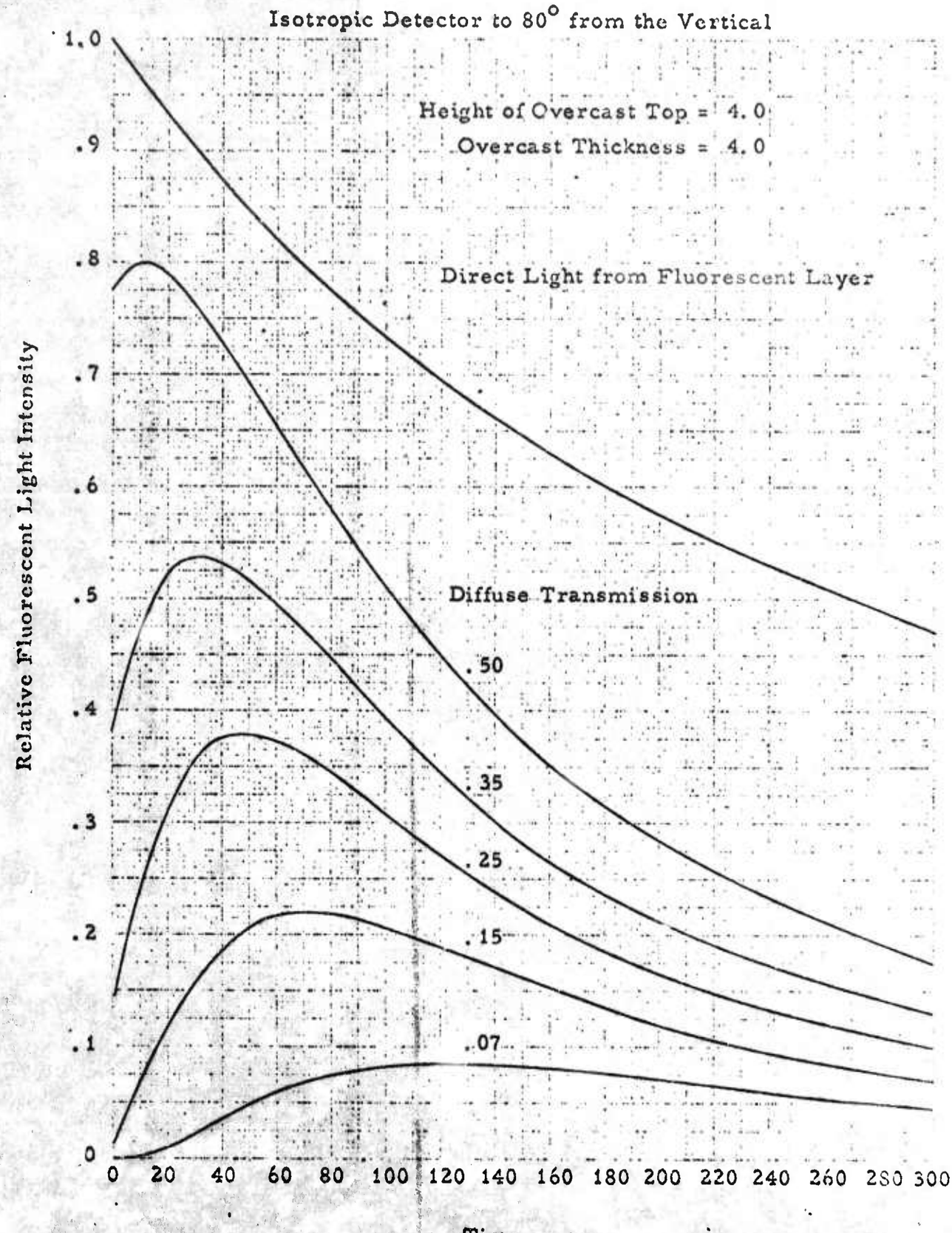

Figure 10

Relative Fluorescent Light Intensity vs. Time

For an Overcast of Various Diffuse Transmissions

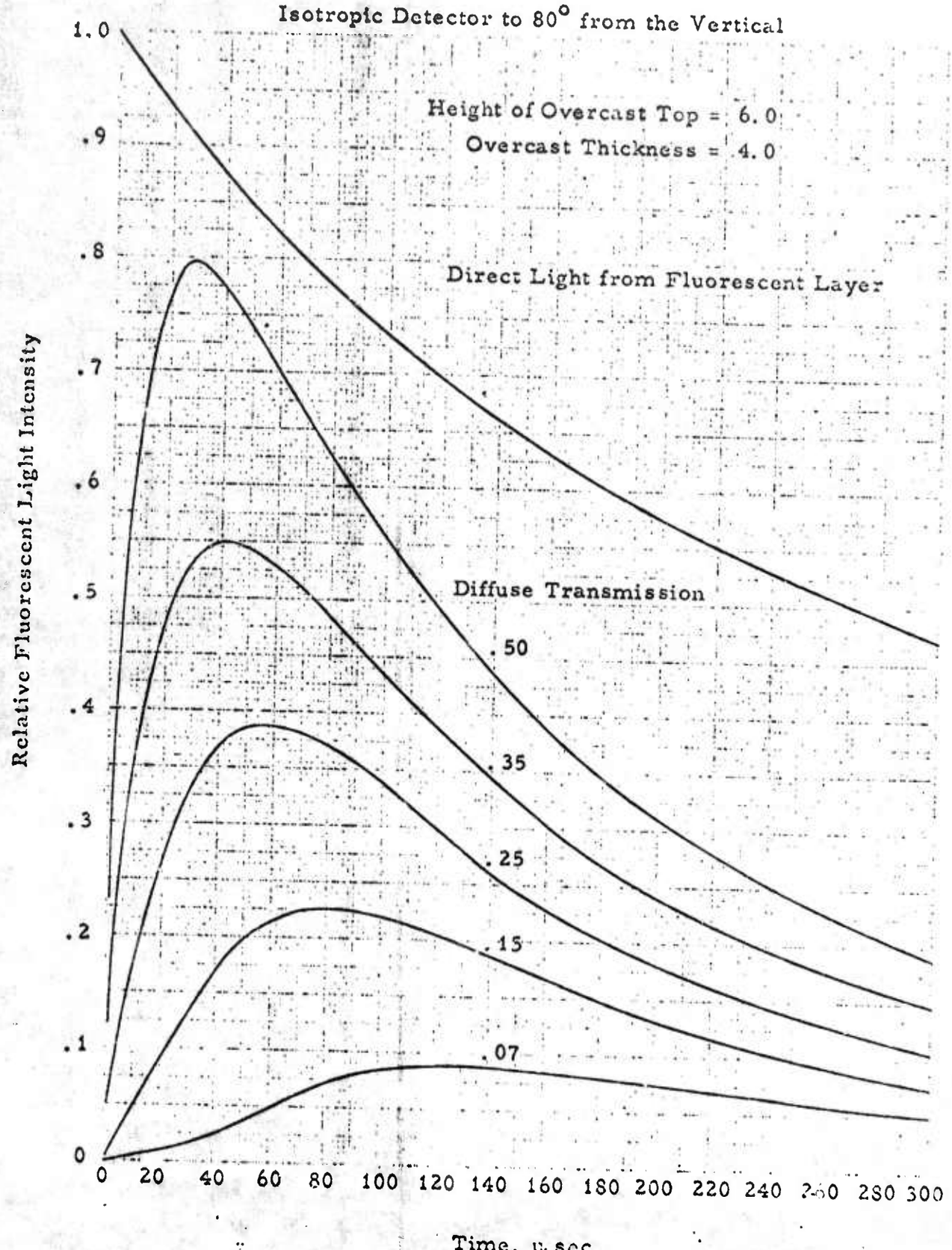

Figure 11

Relative Fluorescent Light Intensity vs. Time

For an Overcast of Various Diffuse Transmissions

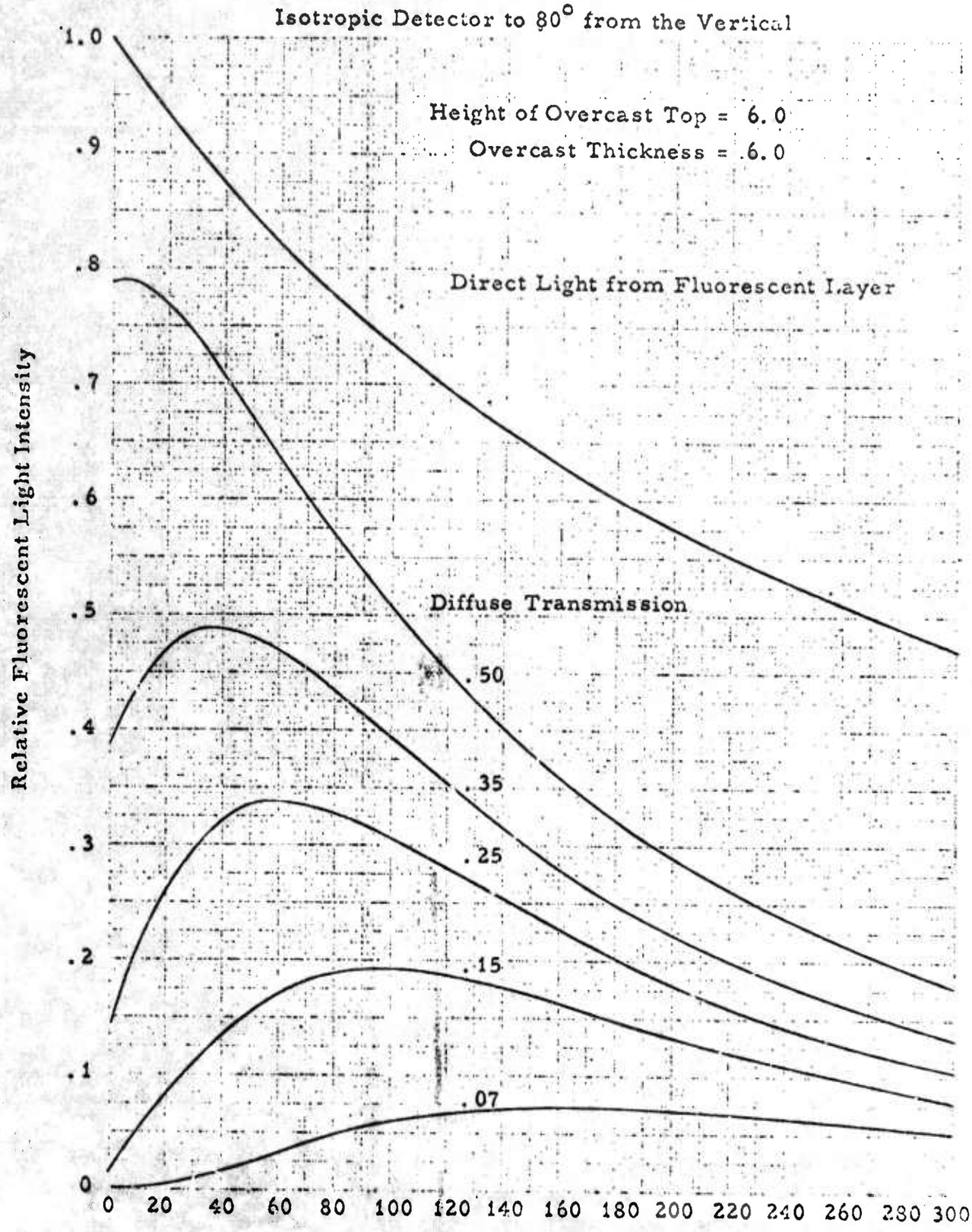

APPENDIX C

On Scintillation and Atmospheric Turbulence

by G. Milne

1. Scintillation of apparently small light sources (stars or distant terrestrial sources) results from optical path variations apparently due primarily to thermal inhomogeneity of the intervening medium. For horizontal paths these inhomogeneities are normally distributed more or less uniformly along the line of sight, and the resultant degradation of optical imagery may be dealt with fairly well on the basis of statistical models. For vertical paths the situation is rather different, the most significant difference undoubtedly being the considerable degree of stratification which is normally present. The various air layers in the line of sight are not readily accessible, so that their properties must be inferred from observations which must usually be made on the ground. Assuming that at least a large part of the scintillation observed in the case of a star arises from a single disturbed layer at a considerable altitude, the velocity (including speed and direction) of such a layer may in principle be inferred from correlation of observations with two telescopes separated by a known distance. Further, the apparent angular velocity of such a layer may be determined from correlation of observations of two stars of known angular separation, from which, knowing the linear velocity, the altitude of the layer may be found. In practice these observations turn out to be very difficult, due in part to signal-to-noise problems associated with the low radiant energy density available from stars, but primarily due to the nature of this turbulence, since the lifetimes of individual segments of the spatial turbulence pattern are of the same order as

the time required for them to move their diameter, so that quite sophisticated correlation techniques are required, with long times of observation. Reasonable progress has nevertheless been made in this direction. To my knowledge, no actual measurements of apparent angular velocity have been made. It has long been observed that double stars scintillate together, indicating that for separations of the order of a few seconds of arc any correlation time interval must be very small, which is in agreement with other crude observations of my own, mentioned below. The distribution of adequately bright stars is not favorable for such observations, so that on the whole the use of stars for atmospheric turbulence measurements seems of rather limited value.

2. There still seems to be a need for a great deal more observation of scintillation for vertical paths, with an effort to relate these to current theories on turbulence, and perhaps relate it quantitatively with variations in temperature or other quantities. Probably the most significant contribution that could be made as an initial step would be the determination of velocity and altitude for turbulent layers and possible association of these with regions of shear such as the tropopause. In this connection, further consideration might be given to variations of longer period, of the order of 0.1 second to several seconds, and one means of approaching this might be by direct observation of schlieren effects on the limb of the sun, moon or planets. While such observations are strictly not identical with scintillation observations, they are similar, and would appear to provide a valid approach

to the obtaining of data on physical conditions of the atmosphere overhead. Rough estimates of the velocity of atmospheric disturbances along the limb of the sun and moon indicate values of angular velocity in the order of several minutes of arc per second, and in the case of the moon some correlation has been observed between this angular velocity and movements of shadow bands for stars in the same part of the sky. Observations might be made either photo-electrically or photographically, and, with appropriate correlations, the opportunity exists for obtaining both velocity and altitude of turbulent layers. Furthermore, in addition to the advantage of greater available energy, there is also the possibility of obtaining data during the daytime as well as at night, which would be very difficult if only stars are used. Since the time resolution required may severely limit exposure time in photographic observations, it is possible the use of image orthicons might be valuable here. Such observations would include simultaneous viewing with two separated apertures.

3. There may be interesting possibilities in correlating results of vertical ranging with observations of celestial objects near the horizon since evidence of atmospheric stratification may be frequently seen here. Such observations might be made on the sun, moon, planets, and even satellites such as Echo I and II, but knowledge of atmospheric refraction may not be adequate for obtaining quantitative information.

4. While interest in stellar scintillation has come about chiefly in connection with astronomical observation, and more recently in connection with "seeing" from high altitude, the most important

significance of turbulence observations might well lie in the field of meteorology, particularly if reasonably simplified observation techniques can be developed which would permit simultaneous observations from a number of stations. It should be possible to follow such phenomena as jet streams, and perhaps more subtle fluctuations in air mass movements. The limitations of optical wave lengths under cloud cover would make it desirable to work at other "windows" at longer wave lengths, but this would undoubtedly be very difficult.

5. In connection with (2), it might be of considerable interest to check correlations with time-lapse photography (or similar observations) on light cloud cover such as cirrus, altocumulus, and perhaps even jet contrails. Strong turbulence may frequently be seen associated with scattered cumulus-type cloud cover at night.

APPENDIX D

ATMOSPHERIC SCINTILLATION OF AN EXTENDED SOURCE

by Wendell A. Horning and J. J. McClure

1. Statement of Problem

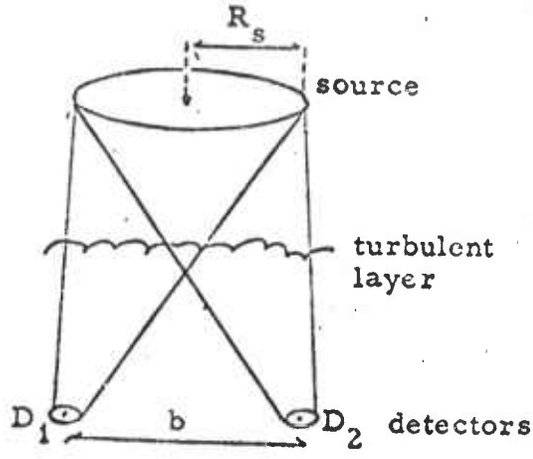

Figure 1

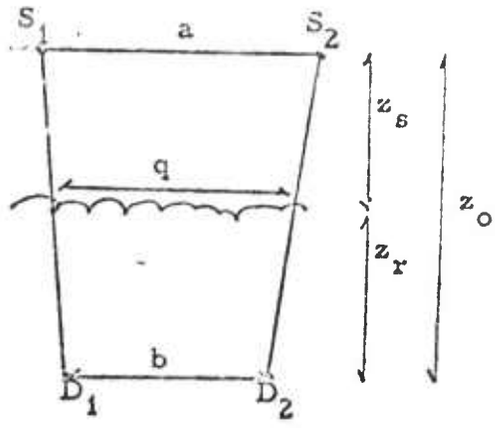

Figure 2

A detector D_1 is considered to view the sun or a planet through the atmosphere. The detector output is taken to be proportional to the integral of light intensity over the detector area. Even if the light source is steady, detector output will vary randomly as a result of atmospheric turbulence. It is desired to calculate the variance of the fluctuations in this output, their spectral density, as well as their correlation length. If two pencils of light cross the turbulent layer at two positions separated by a distance q smaller than the scale length w of the turbulence, they suffer amplitude and intensity changes which are correlated, while there may be negligible correlation if $q >> w$. Thus, there is a statistical correlation between the outputs of two detectors, to be calculated as a function of their separation, b.

It will turn out that fluctuations in detector output are sensitive to both the size and the shape of an extended source. A description will be given of a method for deducing at least the gross features of source

size and shape from an analysis of these fluctuations. A second use for knowledge of turbulence produced fluctuations is in the design of experiments to measure the altitude distribution of turbulence, which is at present not known in detail. More knowledge of this distribution would contribute to the safety of jet aircraft and would be of use in studies of weather, as well as in the design of optical systems.

2. The Case of Two Point Sources and Two Point Detectors

The problem of Section 1 can be approached through a simpler problem, as illustrated in Figure 2. S_1 and S_2 are two point sources of light separated by distance a, and at distance z_s from the turbulent layer. D_1 and D_2 are point detectors separated by distance b, and at a distance z_r from this layer. Light from S_1 may reach D_1 by the path S_1D_1 to produce a displacement in the optical field of the form $A_{11}e^{iS_{11}}$, where A_{11} and S_{11} are an amplitude and a phase. The total displacement at D_1 resulting from the two sources will be

$$\phi_1 = A_{11}e^{iS_{11}} + A_{12}e^{iS_{12}} \tag{1}$$

The similar displacement at D_2 will be

$$\phi_2 = A_{21}e^{iS_{21}} + A_{22}e^{iS_{22}} \tag{2}$$

A path such as S_1D_1 may be formally called a ray, but we do not mean to exclude effects of diffraction.

The power J_1 reached at D_1 will be $\phi_1\phi_1^*$, where a star indicates a complex conjugate. Or,

$$J_1 = A_{11}^2 + A_{12}^2 + 2A_{11}A_{12}\cos(S_{11}-S_{12}) \tag{3}$$

If the light sources S_1 and S_2 are incoherent, as is assumed, then the phases S_{11} and S_{12} will be uncorrelated, and the cosine term in (4) may then be ignored. Intensities at a single detector will now be additive, or

$$J_1 = J_{11} + J_{12}\,,\quad J_2 = J_{21} + J_{22} \tag{4}$$

where J_{11}, for example, is an abbreviation for A_{11}^2. Correlations between two quantities such as J_{11} or J_{12} or between J_{11} and J_{21} may not, however, be ignored. The essence of the problem consists of taking such correlations into account in the proper way.

Let j_1 and j_2 be the fluctuations in the output of detectors 1 and 2. Let j_{11} be the fluctuation in that portion of the output of detector 1 produced by light from source 1, as shown in Figure 2, and so on. Then,

$$\begin{aligned} j_1 &= j_{11} + j_{12} \\ j_1^2 &= j_{11}^2 + j_{12}^2 + 2 j_{11} j_{12} \end{aligned} \tag{5}$$

Write

$$\begin{aligned} &\sigma_1^2 \equiv \overline{j_1^2}\,,\quad \sigma_{11}^2 \equiv \overline{j_{11}^2}\,,\quad \sigma_{12}^2 \equiv \overline{j_{12}^2} \\ &R_{11,12} \equiv \overline{j_{11} j_{12}} \end{aligned} \tag{6}$$

In (6) the bar indicates a statistical average which may be taken as a time average since the random properties of the turbulence are assumed to be stochastic. The symbol σ indicates the variance of some quantity. σ_1, for example, is the variance or rms value of the fluctuations in the output of detector 1. σ_{11} is the variance of that portion of the output of detector 1 which arises from source 1, and so on. The symbol R in (6) indicates the average of the product of two fluctuations, and is called the correlation between these fluctuations. By (5) and (6)

$$\sigma_1^2 = \sigma_{11}^2 + \sigma_{12}^2 + 2\,R_{11,12} \tag{7}$$

which is the rule for finding the variance σ_1 of the sum of the two fluctuations j_{11} and j_{12} which may be correlated. The correlation

between the total fluctuations of detectors 1 and 2, in the above notation, will be

$$R_{12} \equiv \overline{j_1 j_2} = \sum_{\mu=1}^{2} \sum_{\nu=1}^{2} R_{1\mu,2\nu} \tag{8}$$

a summation which is easily extended to the case of a source composed of many discrete points. It is customary to define the correlation coefficient ρ between two quantities, say j_{11} and j_{12}, by the equation

$$\rho_{11,12} = R_{11,12}/\sigma_{11}\sigma_{12} \tag{9}$$

This dimensionless quantity ρ must lie between - 1 and + 1. If the various point sources are of equal strength and if the turbulence is statistically uniform in space, then $\sigma_{11} = \sigma_{12} = \cdots = \sigma$, and (9) may be written

$$R_{12}/\sigma^2 = \sum_{\mu\nu} \rho_{1\mu,2\nu} \tag{10}$$

3. Extended Source

If the source covers an area A, but the detector at D_1 has a diameter small compared to the scale length of the turbulence, then the total fluctuation of the output of D_1 is given by the new formula

$$j_1 = \int_A j_1(\bar{s})\, d\bar{s} \tag{11}$$

$\bar{s}$ indicates position on the source, and $d\bar{s}$ is an element of source area A. Now, $j_1(\bar{s})\, d\bar{s}$ is a distinct random variable for each distinct element of area $d\bar{s}$. These variables are infinite in number and correlated. Their joint probability distribution is hence infinitely dimensional, but the usual statistical averages may still be taken. The square of j_1 may be expressed by the double integral

$$j_1^2 = \int_A \int_A j_1(\bar{s}) j_1(\bar{s}')\, d\bar{s}\, d\bar{s}' \tag{12}$$

The variance of j_1 will then be

$$\sigma_1^2 \equiv \overline{j_1^2} = \int_A \int_A R_1(\bar{s}, \bar{s}')\, d\bar{s}\, d\bar{s}' \tag{13}$$

where $R_1(\bar{s}, \bar{s}')\, d\bar{s}\, d\bar{s}'$ is the unnormalized correlation between those two contributions to fluctuations at the detector D_1 which arise from area elements $d\bar{s}$ and $d\bar{s}'$. The form of the function $R_1(\bar{s}, \bar{s}')$ is deducible from Tatarski. If the source area is of uniform brightness and if the source diameter subtends only a small fraction of a radian at the detector, then R_1 is a function of $|\bar{s}-\bar{s}'|$. If the limb darkening of the sun is to be treated, then R_1 may be written approximately

$$R_1(\bar{s}_1, \bar{s}_1') \simeq G(\bar{s}) R_u(|\bar{s}-\bar{s}'|) \tag{14}$$

where R_u is the form for R_1 when the limb darkening is ignored and $G(\bar{s})$, unity at the sun's center, is the fractional darkening as the source point moves toward the sun's edge. Equation (14) is quite good for the sun, because in the symbols of Figure 2,

$$D_s/z_o << w/z_r$$

where D_s is the sun's diameter and $w = 10$ cm is the scale length for atmospheric turbulence. That is, within a correlation length projected to the sun, its brightness changes by a very small fraction.

To compute the correlation R_{12} between the outputs of the two point detectors, we write for these outputs

$$j_1 = \int j_1(\bar{s})\, d\bar{s}, \quad j_2 = \int j_2(\bar{s})\, d\bar{s} \tag{15}$$

For each infinitesimal pencil of light from source to detector there is a distinct random variable. Two pencils are the same only if they start from the same source area element and end on the same detector.

The result is

$$R_{12} = \int_A \int_A R_{12}(\bar{s}, \bar{s}')\, d\bar{s}\, d\bar{s}' \tag{16}$$

in which $R_{12}(\bar{s}, \bar{s}')\, d\bar{s}\, d\bar{s}'$ is the unnormalized correlation between increments of the detector power which may or may not arise from the same source area element, but which must be delivered to distinct detectors. As in the similar result (13), the function R_{12} depends only on $\bar{s}-\bar{s}'$ if the source is uniform in brightness. If not, a limb darkening function may usually be introduced as in (14).

If the two detectors at D_1 and D_2, as well as the source, extend over significant areas, then the fluctuation of the output from an area element dr_1 of D_1 is $j_1(\bar{r}_1)\, d\bar{r}_1$. The total fluctuation at D_1 will be $j_1 = \int_{B_1} j_1(\bar{r})\, d\bar{r}$, where B_1 is the sensitive area of D_1. The variance of j_1 will be σ_1, given by

$$\sigma_1^2 = \int_A ds \int_A ds' \int_{B_1} dr \int_{B_1} dr'\, R(\bar{r}, \bar{s}, \bar{r}', \bar{s}') \tag{17}$$

where $R(\bar{r}, \bar{s}, \bar{r}', \bar{s}')\, d\bar{r}\, d\bar{s}\, d\bar{r}'\, d\bar{s}'$ is the unnormalized correlation between an element of the power to D_1 which flows from $d\bar{s}$ to $d\bar{r}$ and a second such element which arises from $d\bar{s}'$ and is delivered to $d\bar{r}'$. σ_2^2, which applies to the detector D_2, is given by (17) after the subscript 1 is replaced by 2. If the source is of uniform brightness over its area and if both source and detector diameters subtend only a small fraction of a radian at the turbulent layer, then the function R of (17) can be simplified to the form

$$R \simeq R(|\bar{r}-\bar{r}'|, |\bar{s}-\bar{s}'|, \phi)$$

where ϕ is the azimuth angle between the vectors $\bar{r}-\bar{r}'$ and $\bar{s}-\bar{s}'$. Limb darkening may be introduced as before.

A derivation similar to that for (17) shows that the correlation between outputs of the two extended detectors D_1 and D_2 is

$$\sigma_{12} = \int_A d\bar{s} \int_A d\bar{s}' \int_{B_1} d\bar{r} \int_{B_2} d\bar{r}' \, R(\bar{r}, \bar{s}, \bar{r}', \bar{s}') \tag{18}$$

where B_1 and B_2 are the sensitive areas of the two detectors.

4. Correlation Between Two Narrow Beams

The central diffraction maximum produced by an eddy of size w will have an angular half width of λ/w, where λ is the wave length of light, this from elementary principles. Suppose w is so small that λ/w is large compared to the angle subtended by w at the detector on the ground. Then, where z_r is altitude of the turbulence,

$$\lambda/w \gg w/z_r \tag{19}$$

If (19) is satisfied by w, then the diffraction patterns of most eddies will overlap at the point detector, and there will be statistical cancellation of their fluctuations at the detector even though this cancellation will not be complete. If, on the other hand,

$$\lambda/w \ll w/z_r$$

then at any given time the diffraction pattern of only one eddy of size w will significantly affect the detector, and small changes in its central position will but little affect the fluctuations of detector output. Hence, intuitively, eddy sizes which satisfy

$$\lambda/w \simeq w/z_r , \quad w \simeq (\lambda z_r)^{1/2} \tag{20}$$

will make the chief contribution to detector fluctuations, a result which agrees with a more rigorous discussion. This assumes, of course, that z_r is sufficiently large so that the detector is in the diffraction zone, not the geometrical optics zone. In practice, this means that z_r is greater than a few hundred meters, which includes the cases of present interest. Hence, the correlation length of fluctuations at the ground will be of the order of $(\lambda z_r)^{1/2}$.

A detailed correlation coefficient $\rho(r)$ for fluctuations at the ground and from a point source is given by Tatarski on p. 154 (Ref. 1) for the case where the turbulence is of uniform intensity from the ground to an altitude L. It may be fitted quite well by a function of form

$$\left.\begin{aligned} \rho(r) &= c_1 \exp(-r^2/u_1^2) - c_2 \exp(-r^2/u_2^2) \\ c_1 &> c_2 , \quad u_1 < u_2 \end{aligned}\right\} \tag{21}$$

It has the important property

$$\int \rho(r)\, d\bar{r} = 0 \tag{22}$$

where the integration is over all the horizontal plane through the detector. Equation (22) is equivalent to the assumption that the turbulent atmosphere is non-absorbing and is a sufficiently weak scatterer so that all the light which falls on it from above ultimately falls somewhere on the ground. The effect of the turbulence is then only to redistribute the light on the ground. With this assumption,

$$\int j(\bar{r})\, d\bar{r} = 0 \tag{23}$$

where $j(\bar{r})$ is the intensity fluctuation as a function of ground position of the light from any source. By definition $\rho(r)$ is the time average of $j(\bar{r}_1) j(\bar{r}_1 + \bar{r})$, where r_1 is any ground position. If the turbulence has statistical properties unchanging with time, then by the ergodic theorem we have

$$\rho(r) = \int j(\bar{r}_1) j(\bar{r}_1 + \bar{r})\, d\bar{r}_1 \tag{24}$$

where the integration is again over the ground plane. Integrating (24) and using (23) yields (22). It follows from (22) that the constants of (21) must satisfy

$$c_1 u_1^2 - c_2 u_2^2 = 0 \tag{25}$$

A form of the intensity correlation coefficient more general than (21) is

$$\rho(q) = c_1 \exp(-q^2/u_1^2) - c_2 \exp(-q^2/u_2^2) \qquad (26)$$

where $\rho(q)$ is the correlation between the intensity from a source S_1 at a detector D_1 and the intensity from a source S_2 at a detector D_2, and where q is the distance between the two intersections of lines S_1D_1 and S_2D_2 with a thin layer of turbulence (see Figure 2). Tatarski's plot of ρ applies strictly to a uniform layer of turbulence extending from the ground to a height L. For the present we consider it to hold also for a thin layer at height L/2. Then approximate values of the constants of (26) may be obtained by fitting his curve. A more complete derivation of the constants of (26) along with a fit to ρ possibly containing more than two terms will be given later.

5. Source Extended in One Dimension

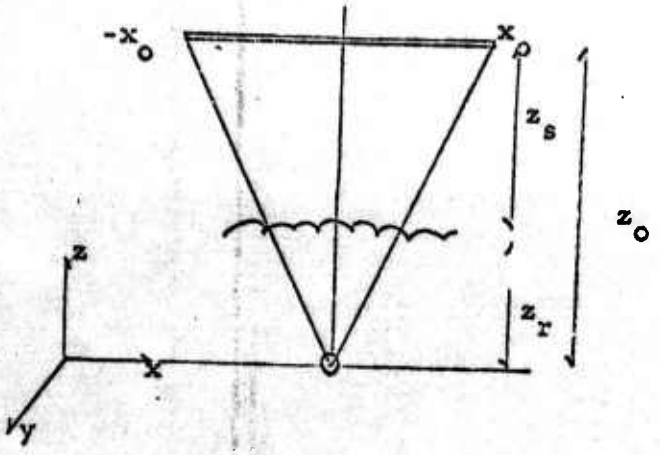

Figure 3

As a helpful preliminary problem, consider a line source of light $2x_o$ at distance z_o from a detector D, as in Figure 3. Light from the source traverses a thin layer of turbulence at height z_r. According to Sections 3 and 4, the variance σ in the detector output

will be given by

$$\left.\begin{aligned} \sigma^2 = \int_{-x_o}^{x_o} dx \int_{-x_o}^{x_o} \Big\{ & c_1 \exp\left[-(x-x')^2/w_1^2\right] \\ & - c_2 \exp\left[-(x-x')^2/w_2^2\right] \Big\} \\ w_1 \equiv u_1 z_o/z_r, \quad & w_2 \equiv u_2 z_o/z_r \end{aligned}\right\} \tag{27}$$

Since the turbulence only redistributes light on the ground, there will be a restriction on the correlation coefficient similar to (25), which in the present two-dimensional problem becomes

$$c_1 u_1 - c_2 u_2 = 0 \tag{28}$$

The first integration of the first term of the integrand of (27) yields

$$c_1 w_1 \int_{-x_o}^{x_o} \left[\operatorname{erf}\left(\frac{x_o - x'}{w_1}\right) + \operatorname{erf}\left(\frac{x_o + x'}{w_1}\right) \right] dx' \tag{29}$$

where

$$\operatorname{erf}(z) \equiv \pm \int_o^z e^{-x^2} dx, \quad z \gtrless 0$$

After the integration over x' is performed, expression (29) becomes

$$c_1 w_1 \left\{ -w_1 \left[1 - \exp\left[-\left(\frac{2x_o}{w_1}\right)^2 \right] \right] + 4x_o \operatorname{erf}\left(\frac{2x_o}{w_1}\right) \right\} \tag{30}$$

The second term of the integrand of (27) yields a similar expression.

If the length $2x_o$ subtends a half degree at the ground, as does the diameter of the sun, and if w_1 and w_2 have sizes appropriate to actual air turbulence, then $2x_o/w_1$ and $2x_o/w_2$ are both of the order of 10^3. Then the exponential terms in σ^2 are negligible. Then the two

erf terms are nearly equal in absolute magnitude and cancel with the aid of (28). The result is

$$\sigma^2 = c_2 w_2^2 - c_1 w_1^2 \tag{31}$$

The rms fluctuation σ at a point detector from a sufficiently extended source is hence independent of source size x_o. The basic reason is that the turbulence only redistributes light from the source. The fluctuations hence result from the source ends and represent an end effect. We will see later that fluctuations from an extended two dimensional source, similarly, represent an edge effect.

6. Source Extended in Two Dimensions

Now consider the line source of Figure 3 replaced by a rectangle with sides of length $2x_o$ and $2y_o$, and in a plane parallel to the layer of turbulence. If $z_o >> z_r$, then the problem will be essentially unchanged if the source lies on any curved surface area, provided the normal projection of the area on a plane parallel to the turbulence is a rectangle with sides $2x_o$ and $2y_o$. The variance σ at a point detector will now be given by

$$\sigma^2 = \int dx\, dx'\, dy\, dy' \left\{ c_1 \exp\left[-\left((x-x')^2 + (y-y')^2 \right) / w_1^2 \right] - c_2 \exp\left[-\left((x-x')^2 + (y-y')^2 \right) / w_2^2 \right] \right. \tag{32}$$

where the range of integration covers the source area twice. Because of the rectangular source shape, each of the two terms of (32) factors into a product of two expressions, each of the form of (30). Hence, (32) becomes

$$\sigma^2 = c_1 w_1^2 \left(2\pi^{1/2} x_o - w_1\right)\left(2\pi^{1/2} y_o - w_1\right) - c_2 w_2^2 \left(2\pi^{1/2} x_o - w_2\right)\left(2\pi^{1/2} y_o - w_2\right) \tag{33}$$

which again assumes x_o and y_o to be very large compared to w_1 and w_2, so that the source dimensions may simulate those of an object such as the sun. Because of (25), the terms of (33) proportional to $x_o y_o$ will cancel, and the terms linear in x_o and y_o will be dominant. (33) hence becomes

$$\sigma^2 = 2\pi^{1/2}(x_o + y_o)(c_2 w_2^3 - c_1 w_1^3) \tag{34}$$

which is proportional to source perimeter and hence exhibits the variance as an effect characteristic of the source edge.

The result (34) can be put into a form consistent with intuition by writing

$$c_2 w_2^3 - c_1 w_1^3 \simeq c w^3 \tag{35}$$

where c is new constant of the order of c_2 and w is of the order of the scale of turbulence increased by the ratio z_o/z_r. w is hence the projection from the turbulent layer to the sun of the scale of turbulence, the projection taken with respect to the point detector. $N = 2(s_o + y_o)/w$ is the greatest number of non-overlapping areas A of size w^2 which can simultaneously touch the edge of the source. Hence, (34) can be put

$$\sigma^2 = NA^2 c, \quad \sigma \simeq \sqrt{N}\, A c^{1/2} \tag{36}$$

The quantity $Ac^{1/2}$ is the variance from a portion of the source of area small enough so that its various parts are well correlated. The factor $\sqrt{N}$ then arises naturally from the usual rule for adding the effect of statistically independent fluctuations. Fluctuations at the detector hence arise principally from a strip of width w which borders the perimeter of the source, provided the source dimensions are large compared to w.

For the case of a round source, say the sun, (34) is replaced by

$$\sigma^2 = 2\pi^{3/2} R_s (c_2 w_2^3 - c_1 w_1^3) \tag{37}$$

where R_s is the source radius.

7. Correlation with an Extended Source

The aim of this section is to compute the correlation σ_{12} between fluctuations of the outputs of two point detectors on the ground, separated by a distance b. The source, as in the preceding section, is a rectangle with sides $2x_o$ and $2y_o$. For the present the line of centers of the detectors is taken parallel to the side of the rectangle of length $2x_o$. Then

$$\sigma_{12} = \int dx\, dy\, dx'\, dy' \left(c_1 \left[\exp -\left\{ (x-x'+\bar{x})^2 + (y-y')^2 \right\} / w_1^2 \right. \right. \left. \left. - c_2 \exp \left[-\left\{ (x-x'+\bar{x})^2 + (y-y')^2 \right\} / w_2^2 \right] \right) \quad (38)$$

$$\left(\bar{x} \equiv \frac{z_s}{z_r} b \right)$$

is the desired quantity, where the meaning of lengths z_r and z_s is given in Figure 2. The integral over x of the first term of the integrand of (38) yields

$$c w_1 \left[\operatorname{erf}\left(\frac{x_o - x' + \bar{x}}{w_1} \right) + \operatorname{erf}\left(\frac{-x_o - x' + \bar{x}}{w_1} \right) \right] \quad (39)$$

The integral of (39) with respect to x' and over the range $-x_o < x' < x_o$ yields

$$I_{1x} = w_1 \left\{ -w_1 \exp\left[-(\bar{x}/w_1)^2 \right] - 2\bar{x} \operatorname{erf}(\bar{x}/w_1) + (2x_o + \bar{x})(\pi^{1/2}/2) + (2x_o - \bar{x}) \exp\left[-\left(\frac{2x_o - \bar{x}}{w_1} \right)^2 \right] + (w_1/2) \exp\left[-\left(\frac{2x_o - \bar{x}}{w_1} \right)^2 \right] \right\} \quad (40)$$

Similarly, the integral of the first term of the integrand over y and y', both over the range $-y_o$ to $+y_o$, yields

$$I_{1y} = w_1 \left(-w_1 + 2\pi^{1/2} y_o \right) \quad (41)$$

which is what (40) becomes when $\bar{x}$ is put equal to zero and x_o is replaced by y_o. Hence (38), fully evaluated, is

$$\sigma_{12} = c_1 I_{1x} I_{1y} - c_2 I_{2x} I_{2y} \tag{42}$$

In (42) the terms proportional to $x_o y_o$ all cancel because of (25). If $\bar{x}$ is very small compared to x_o and y_o, then the terms linear in x_o and y_o dominate. But in general, terms linear in the three quantities x_o, y_o and $\bar{x}$ are of the same order even for a very large source. A plot of (42) has the character shown in Figure 4.

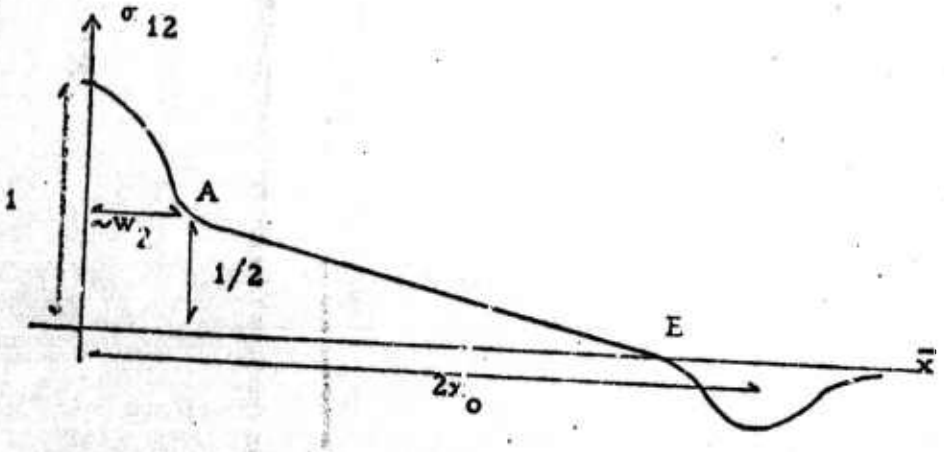

Figure 4

If the line of centers of the two detectors, contrary to what was assumed above, makes any significant angle with the sides of the rectangular source, then the two integrals I_{1x} and I_{1y} become of symmetrical form and the plot of σ_{12}, then appears as in Figure 5.

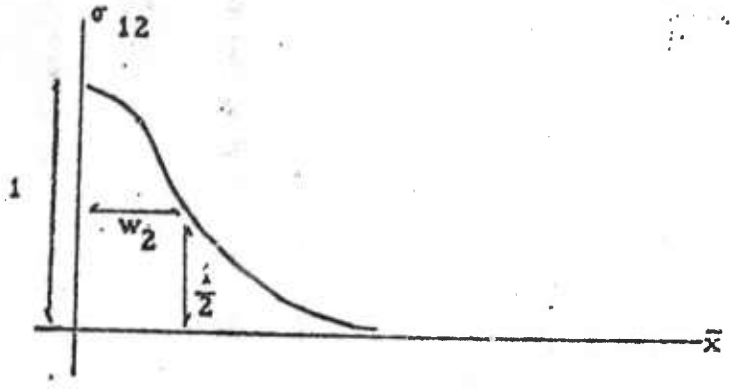

Figure 5

Hence, the character of σ_{12} as a function of $\bar{x}$ is sensitive to the angle between the line of centers of the detectors and the sides of the rectangular source. This can be interpreted by considering the projection of the source on the layer of turbulence, first with respect to detector D_1 and with respect to D_2. If these projections are as in Figure 6a where $w < w_1$, then the correlation is near unity, as

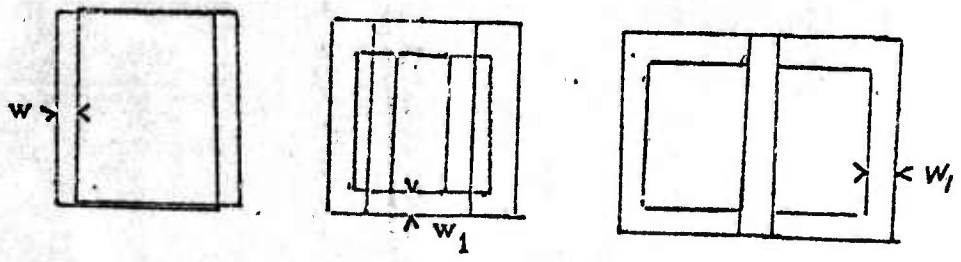

Figure 6

as shown by the peak of Figure 4, for $\bar{x} < w_1$. If the projections are as in Figure 6b, then the correlation is as shown in Figure 4 between A and B. The correlation is then proportional to the degree of overlap

of strips of width $\sim w_1$ along the edges of the two projections. These overlapping strips, as $\bar{x}$ increases, move like the slides of a trombone. If finally the projections are as in Figure 6c, then turbulence in the range of strip overlap will deflect light into one detector when it deflects light out of the other, which gives rise to the anti-correlation shown in Figure 4 for $\bar{x} \sim 2x_o$.

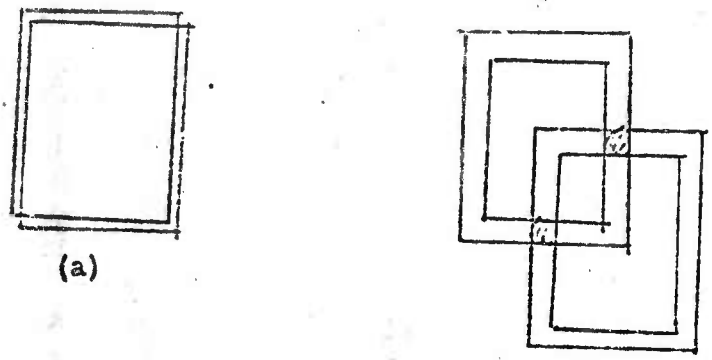

Figure 7

When the line of centers of the detectors is quite non-parallel with the source sides, then the projections of interest are as shown in Figure 7. There is then no extensive overlap of the edge strip which yields the correlation. The trombone effect is then absent, and correlation varies with detector separation as shown in Figure 5.

From the above results for a rectangular source, it is possible to closely estimate the correlation as a function of detector separation when the source is the sun. In this case, when the projections of the sun are as in Figure 8a, with $w < w_1$, then σ_{12} varies with $\bar{x}$ essentially as in Figure 5. But because of the circular nature of the sun, σ_{12} will fall off somewhat less rapidly for $w > w_1$ than in Figure 5. When the projections of the sun on the turbulent layer are as in Figure 8c, the correlation will be essentially zero. When the solar projections are as in Figure 8c, there will be a slight anti-

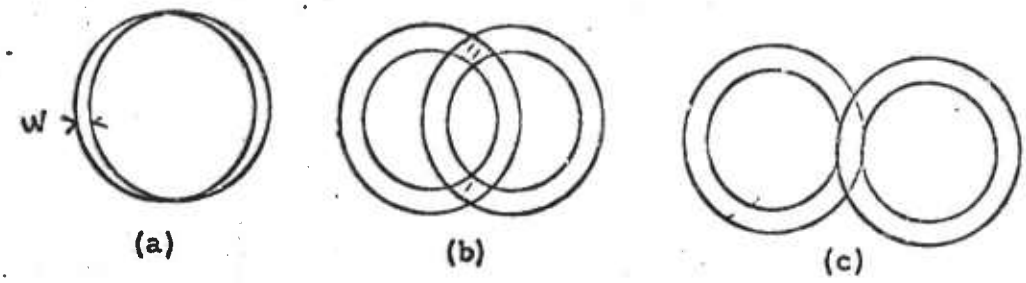

Figure 8

correlation proportional to the shaded area in 8c, but not so prominent as if the source were square with two sides parallel to the line of centers of the detectors.

The above discussion shows that the anticorrelation which occurs for a rectangular source with specially placed detectors, or to a lesser degree with the sun, depends on the height of the turbulence. In fact, the observation of the detector separation at which the anticorrelation occurs can be used in principle to measure the distribution in altitude of turbulence. If a square light source were carried on a high altitude balloon and observed from the ground, the method might be useful if the distribution of turbulence were sufficiently simple, that is, if it consisted principally of only two or three well defined layers.

When light from the sun falls on two nearby small detectors, the correlation between fluctuations in their outputs, as a function of their separation, will be a single hump of half width of the order of $\sqrt{\lambda L}$ where L is the mean height of the turbulence. Equipment of very great accuracy could in principle show the details of the edge of this hump, associated with the circular nature of the solar source, and could in principle show the anticorrelation when the angle subtended at a point in the turbulence by a line between the sources becomes equal to the angle subtended at a point in the turbulence by a solar diameter.

8. The Absolute Value of Fluctuations

The preceding sections, except for a factor, solve the problem of the correlation of fluctuations in detector currents produced by the light from an extended source. The results have been expressed in terms of a correlation coefficient $\rho(t)$, which is unity when the detector separation b is zero. To be complete, these results must all be multiplied by P, the rms value of the fluctuations per unit area of detector, when the source is so small that $\rho(b) \sim 1$ where b is equal to a source diameter. Of course, they must also be multiplied by detector area B to give proper absolute values.

The value of P can be computed from formula (4.18) of Ref. 1, namely,

$$dS = \frac{ck^4 A_o^2 \sin^2\chi}{4z_r^2} \phi_n(\bar{k}-k\bar{m})dV \tag{43}$$

where dS is the mean scattered intensity at distance z_r from a volume dV containing turbulent eddies of air. c is the velocity of light, $\bar{k}$ the incident propagation vector, $\bar{A}_o$ the electric field in the incident light beam prior to scattering by turbulence, while $\bar{m}$ is a unit vector in the direction from dV to the detector. χ is the angle between $\bar{k}$ and $\bar{m}$. ϕ_n is the Fourier space component of the unnormalized correlation B(r) of the index of refraction $n = 1 + n_1$ within the turbulence. More completely stated

$$B(r) = \overline{n_1(\bar{r}')n_1(\bar{r}'+\bar{r})} \tag{44}$$

where the bar indicates a statistical average, and n_1 is the fluctuation in the index of refraction. Also, by definition of ϕ,

$$B(r) = \int e^{i\bar{\kappa}\cdot\bar{r}}\, \phi_n(\kappa)\, d\bar{\kappa} \tag{45}$$

where $\kappa = 2\pi/\Lambda$ is the length of the wave vector of the spatial Fourier component of n_1 with the wavelength Λ. Tatarski shows that

$$\Phi_n(\kappa) = \frac{\Gamma(8/3)\sin(\pi/3)}{4\pi^2} C_n^2 \kappa^{-11/3} \tag{46}$$

where the Kolmogoroff model of the spectrum of turbulence is used and when C_n^2 expresses the strength of the turbulence. C_n, proportional to the rms value of $n_1(r)$, must be determined from experiment in order to obtain results for an actual atmosphere. Evaluating the numerical coefficients in (46) yields

$$\Phi(\kappa) = 0.033\, C_n^2\, \kappa^{-11/3}, \qquad \kappa_o < \kappa < \kappa_1 \tag{47}$$

The inequality in (5) expresses that there exist eddies of diameter w located in the field of turbulence and whose diffraction half angle λ/w is equal to the angle subtended by the eddy at the detector. The condition is usually satisfied for turbulence in a clear atmosphere.

The value of C_n has been obtained from data on star twinkling under the assumption that turbulence is uniform from the ground to a height of 20 km, with a mean height of 10 km. A consistent value has also been obtained from radar scattering experiments. The result is

$$C_n \simeq 7 \cdot 10^{-9}\, \text{cm}^{-1/3} \tag{48}$$

The value of C_n is related to temperature fluctuations in the air through the equation

$$C_n = 79 \cdot 10^{-6} p C_T / T^2 \tag{49}$$

where p is pressure, T is absolute temperature and C_T is defined by

$$\overline{\left[T(r+r_1) - T(r_1)\right]^2} = C_T r^{2/3} \tag{50}$$

The quantity on the left of (50) is called $D_T(r)$, the structure function of the temperature. A simple algebraic expansion shows

$$D_T(r) = 2\left[\overline{T_1^2} - \overline{T_1(r+r_1)\,T(r)}\right] \tag{51}$$

where $T_1 \equiv T - \bar{T}$ is the temperature fluctuation, and D_T is twice the squared variance minus the correlation of T_1. The value of C_T consistent with (48) is $8 \cdot 10^{-3}$.

The angle χ in (1) is given by

$$\cos\chi = \sin\theta\cos\phi \tag{52}$$

where θ is the angle between the propagation vector and a line connecting the detector to the dV and ϕ is the azimuth of $\bar{A}_o$. Scattering angles are of the order of w/z_r, where w is the scale of turbulence and z_r its altitude. In a clear atmosphere, these are so small that we put $\sin\chi = 1$. By simple geometry

$$\bar{k} - k\bar{m} = 2k \sin\theta/2 \simeq kq/z_r \tag{53}$$

where $\bar{q}$ is distance of dV from the line connecting the source point and the detector. Also, $dV = h\,dq$, where h is the thickness of the turbulent layer. Substituting in (1) yields

$$\frac{dS}{S_o} = \frac{2\pi r^4}{z_r^2}\, 0.033\, C_n^2 \left(\frac{z_r}{kq}\right)^{11/3} h\, 2\pi q\, dq \tag{54}$$

where

$$S_o = A_o^2 c/8\pi$$

is the Poynting vector for unscattered light from the distant source. Strictly, q should be taken as a function of altitude; but for the present we evaluate it at the mean height of turbulence, namely, $z_r \simeq 10$ km.

The quantity (54) is to be integrated over the range $q_o < q < \infty$, where $q_o = (\lambda z_r)^{1/2}$ is the diameter of the smallest eddy which contributes strongly to fluctuations at the detector in the diffraction zone; and where λ is the wave length of light. We have

$$\int d\bar{S} \equiv S, \qquad \int_{q_0}^{\infty} q^{-8/3}\, dq = \frac{3}{5}\,(\lambda z_r)^{-5/6} \tag{55}$$

By (54) and (55)

$$(S/S_o) = \frac{3}{5}\,(2\pi)^{7/3}\, 0.033\, C_n^{\,2} h\, (z_r)^{5/6} \Big/ \lambda^{7/6} \tag{56}$$

We take

$$C_n = 7 \cdot 10^{-9}\,\mathrm{cm}^{-1/3}, \quad h = 20\ \mathrm{km}, \quad z_r = 10\ \mathrm{km},$$

$$\lambda = 5 \cdot 10^{-5}\ \mathrm{cm}$$

Then (14) becomes

$$S/S_o = 1.4 \simeq 1 \tag{57}$$

which says that the light from a star scattered by turbulence into a small detector, such as the eye, is as great as the direct light. Since the scattered light is fluctuating with a zero mean, this corresponds to strong twinkling of a star, which is observed. That it does not appear stronger to the eye than it does may be caused by the eye's persistence of vision ($0 \sim .1$ sec) and the fact that the mean frequency of the fluctuations of the scattered light is about 100 cps except when wind speeds are unusually low. The excess of S/S_o over 1 cannot be taken seriously and even contradicts conservation of energy. The above approximate calculation is correct only to a factor of about 2. In what follows, we take $S/S_o \simeq 1$.

The variance σ of turbulence produced by fluctuations from the sun can now be computed from (37). We take

$$c_1 = 1.1, \quad c_2 = 0.1, \quad w_1 = .23(\lambda z_r)^{1/2}\,(z/z_r)$$

$$w_2 = 1.6\,(\lambda z_r)^{1/2}\,(z_s/z_r)$$

which satisfy

$$c_1 - c_2 = 1, \qquad c_1 w_1^2 - c_2 w_2^2 = 0$$

and which roughly fit the curve of Figure 12 of Tatarski. Then,

$$c_2 w_2^3 - c_1 w_1^3 \simeq .40 (z_r)^{1/2} (z_s/z_r)$$

The ratio of the rms fluctuation to the mean value of the detector output as produced by sunlight is

$$\frac{\sigma}{4\pi R_s^2} = \frac{\left[2\pi^{3/2} R_s (c_2 w_2^3 - c_1 w_1^3)\right]^{1/2}}{4\pi R_s^2} = 9.42 \cdot 10^{-6} \qquad (58)$$

This result holds for a detector whose area is less than the correlation area

$$A_c \simeq .25 \cdot \lambda z_r = 12.5 \text{ cm}^2$$

If detector area is NA_c, where $N > 1$, then the ratio of the mean fluctuation to the average detector output is the number given by (58) divided by $\sqrt{N}$. A more refined result could be obtained if the altitude distribution of the turbulence were better known. If experiment shows fluctuations substantially greater than predicted by (58), it would indicate that the light from the sun is itself fluctuating.

9. Elementary Correlation Coefficient and Results

As already mentioned above, a detailed correlation coefficient for fluctuations at the ground of light received from a point source is given by Tatarski in Reference 1. He obtains a theoretical correlation coefficient (p. 154) and also an experimental one (p. 213), which is reproduced in the upper portion of Figure 9.

An approximation to the experimental curve (solid line) is given in the form of Equation (21) (dash line) with $c_1 = 1.33$, $c_2 = 0.33$, $u_1 = 0.956\sqrt{\lambda L}$ and $u_2 = 1.912\sqrt{\lambda L}$. These numbers assure that the Condition 22 is fulfilled. It should be noted that the experimental curve does not satisfy the Condition 22, which, as discussed above, is necessary when the turbulent atmosphere is non-absorbing and a sufficiently weak scatterer. It is clear, however, that the solid line could be shifted considerably within the indicated experimental error so that the Condition 22 would be satisfied.

The central curve in Figure 9 shows the correlation coefficient for the intensity fluctuations in two point detectors as a function of their separation distance. This is obtained by assuming that the line of separation between the two detectors lies along the diagonal of the assumed square source. It is seen that the half width of the intensity correlation is approximately $\sqrt{\lambda L} \sim 7$ cm.

The "trombone effect" is demonstrated in the lower portion of Figure 9. The change to a logarithmic scale should be recognized. This curve shows the correlation over large distances when the detectors lie on a line corresponding to a side of the square source. This curve demonstrates clearly the edge effects as discussed above. The anticorrelation dip at $b/\sqrt{\lambda L} \sim 2 \times 10^3$ is obtained for a source of solar dimensions and occurs at approximately the distance of the projection of the sun onto the earth's surface through the turbulent layer, ~ 140 m. The width of the central peak and the width of the anticorrelation dip are approximately equal to $\sqrt{\lambda L}$, although at first glance this is not apparent because of the change of scale.

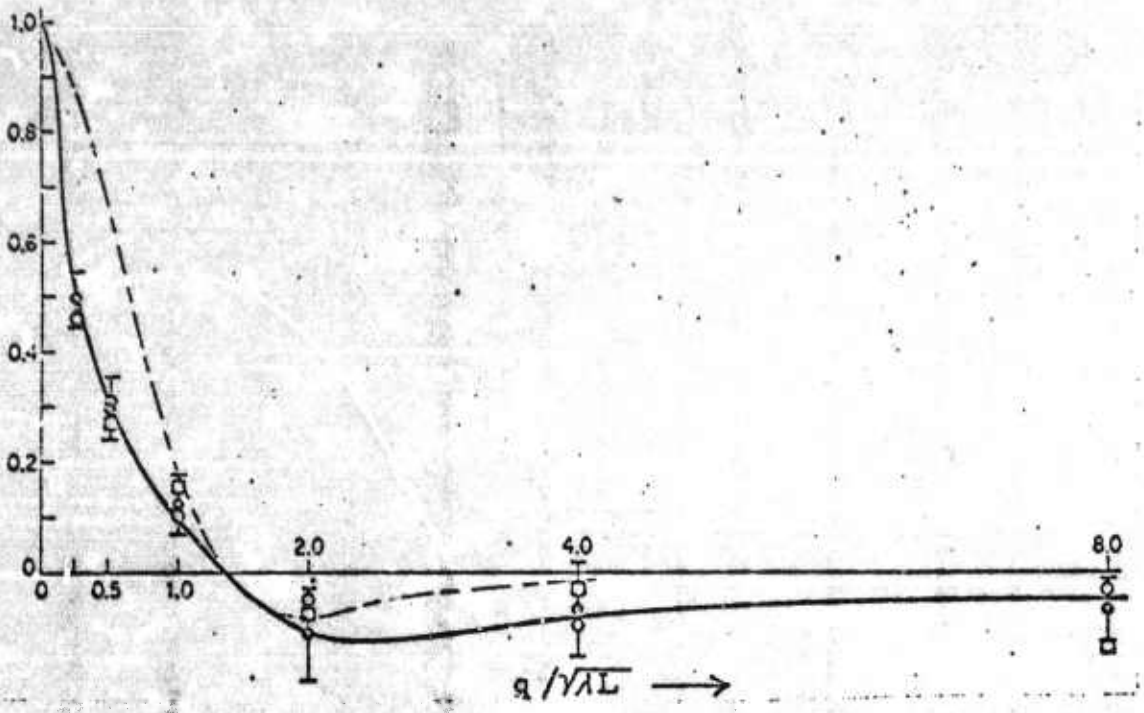

——— Empirical correlation coefficient of the fluctuations of light intensity (Ref. 1).

— — — Approximate correlation coefficient.

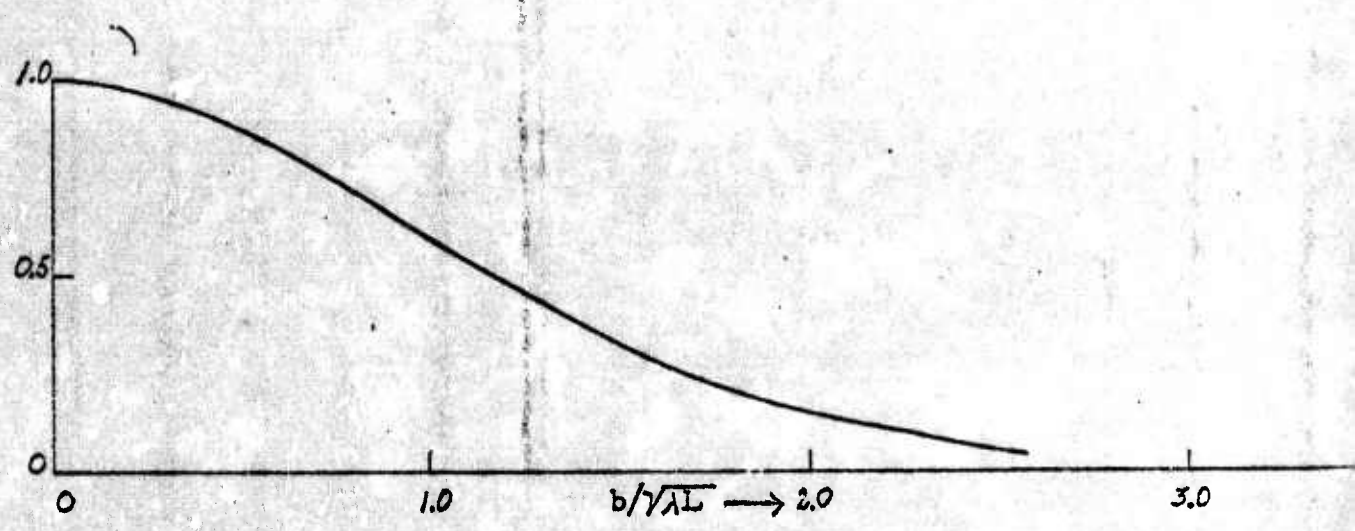

Correlation coefficient for extended source with point detectors along diagonal.

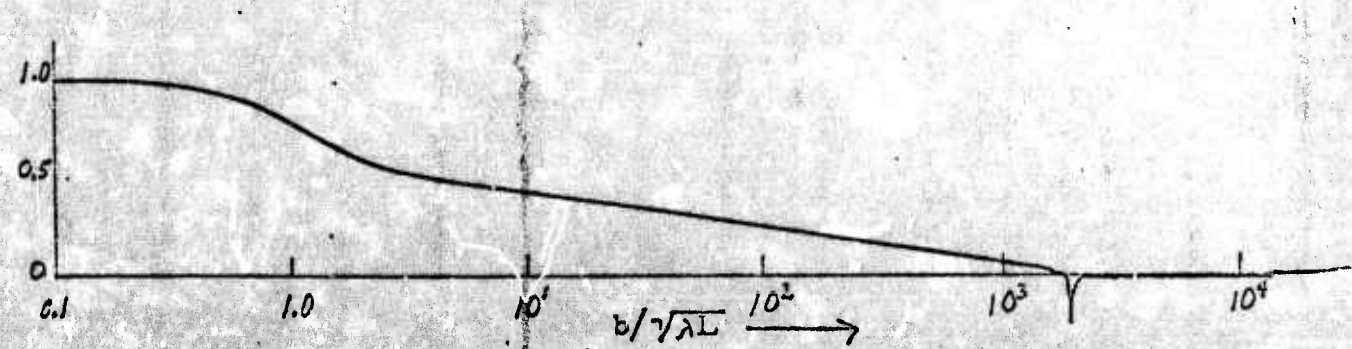

Correlation coefficient for extended source with point detector along edge.

Figure 9

REFERENCES

1. V. I. Tatarski, Wave Propagation in a Turbulent Medium, McGraw-Hill Book Co., Inc., 1961.

APPENDIX E

Experimental Data on Scintillation of Sunlight

By R. Hopfield

We have experimentally studied the fluctuations of sunlight caused by atmospheric scintillation. Preliminary results have been obtained concerning

1. Absolute noise levels due to scintillation.
2. Correlation of signals to separate detectors.
3. Power spectra of the noise.

Some of these studies were made during inversion conditions, a not uncommon situation in the Los Angeles area. The effects of these conditions on the experimental results are not fully understood at the present time. Phenomena not related to the refractive effect of turbulence may affect the results of experiments made under these conditions, i.e., effects such as structured haze blowing by, variations in the water vapor in the path, etc. All quantitative data given were taken with IRC S1020E8-solar cells (area 2 cm^2) individually biased at 10 ohms. Multiple cell configurations were formed by series connection of the biased units.

1. Absolute Noise Levels

The absolute noise levels are given in Table I. The data were taken in the Santa Monica area. Noise level varies considerably from day to day and hour to hour. No attempt has been made to arrive at an average; the figures given in Table I are only representative. The "closed" configuration was a 5 x 5 array of cells with overall dimensions 7 x 10 cm; the "open" configuration also had five cells to a side, but the cells were mounted with a three-inch spacing between centers.

2. Signal Correlation

Figure 1 shows actual unselected scope traces generated by two cells at various separations. The sense of the lower trace is opposite to that of the upper trace, to allow the use of symmetry in evaluating correlation. It is obvious that correlation exists, and that it decreases with increasing detector separation, but we have not yet succeeded in getting any trustworthy numbers in this area. The data shown were taken during inversion conditions.

3. Power Spectra of Scintillation Noise

These were evaluated with a Singer Panoramic Analyzer, Model LP-1A. The measured square bandwidth of the analyzer was about 56 cycles. Figure 2 shows spectral data for the output of 1 and 25 cells; integrated noise in each case corresponds within 30 percent to the total noise at the time measured on a Ballantyne true rms meter. By inspection of Figure 2 it appears that roughly 5×10^{-3} of the total scintillation noise power is in frequencies above 200 cps, the fall-off being a little more than a factor of 10 per 100 cps.

TABLE 1

Absolute Scintillation Noise Levels

Close Array - No Inversion

No. of Cells	Cell Area (cm^2)	DC Voltage	rms Noise (volts)	Noise Power μ watts
1	2	.44	.00042	0.016
4	8	1.68	.0013	0.04
9	18	3.8	.002	0.04
16	32	6.7	.0025	0.039
25	50	10.8	.003	0.036

Open Array - No Inversion

No. of Cells	rms Noise (volts)	Noise Power μ watts
1	.0004	0.016
4	.0012	0.03
9	.0018	0.035
16	.002	0.025
25	.003	0.036

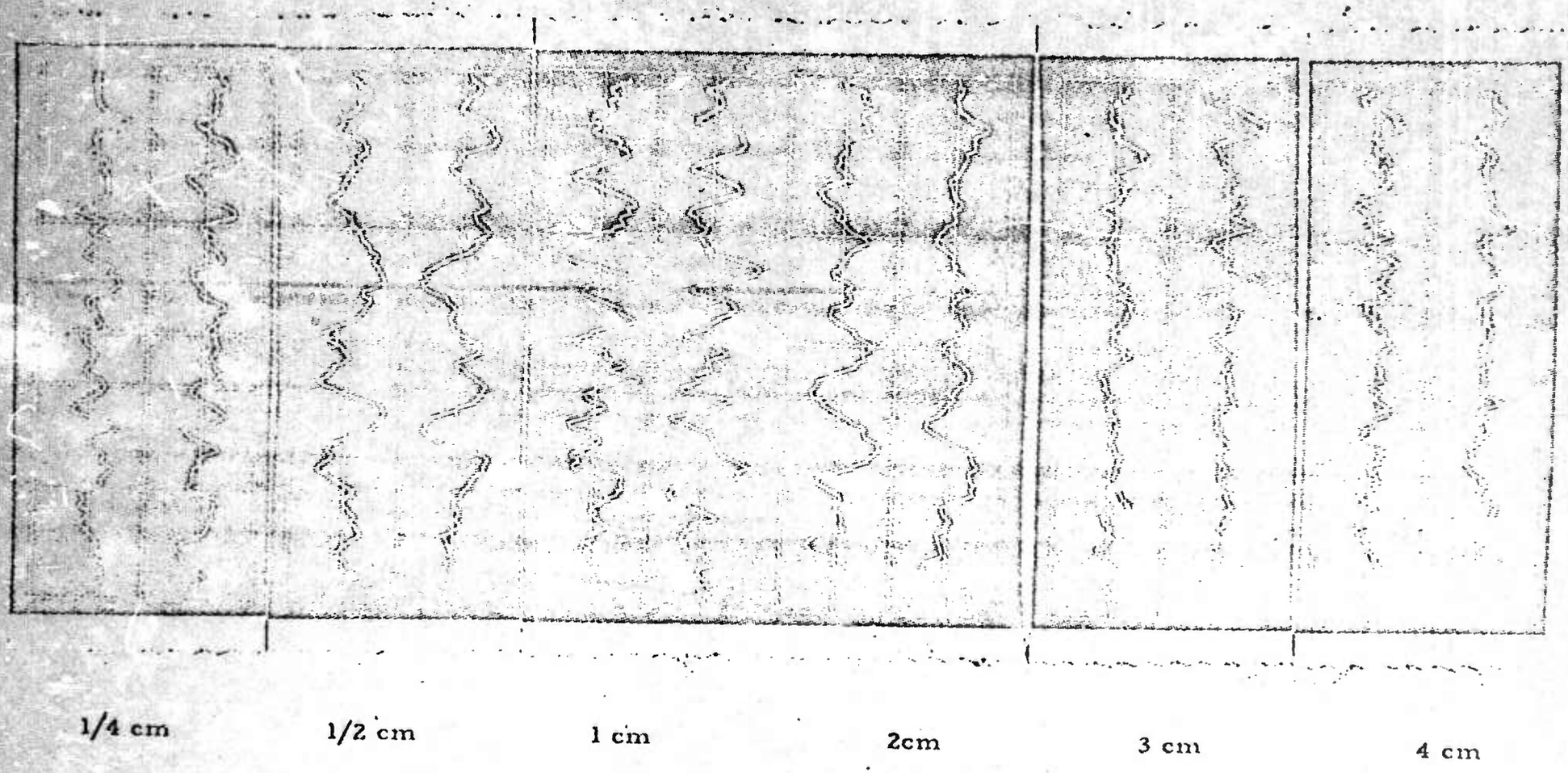

Figure 1

Oscilloscope Traces of Two Detectors at Various Separations

(Taken under inversion conditions where the origin of fluctuations is not fully understood.)

Figure 2

Power Spectra of Scintillation

(Taken under inversion conditions, where the origin of fluctuations is not fully understood.)